# Physics of automated driving in framework of three-phase traffic theory

Boris S. Kerner

*Physics of Transport and Traffic, University Duisburg-Essen, 47048 Duisburg, Germany*

We have revealed physical features of automated driving in the framework of the three-phase traffic theory for which there is *no* fixed time headway to the preceding vehicle. A comparison with the classical model approach to automated driving for which an automated driving vehicle tries to reach a fixed (desired or "optimal") time headway to the preceding vehicle has been made. It turns out that automated driving in the framework of the three-phase traffic theory can exhibit the following advantages in comparison with the classical model of automated driving: (i) The absence of string instability. (ii) Considerably smaller speed disturbances at road bottlenecks. (iii) Automated driving vehicles based on the three-phase theory can decrease the probability of traffic breakdown at the bottleneck in mixed traffic flow consisting of human driving and automated driving vehicles; on the contrary, even a single automated driving vehicle based on the classical approach can provoke traffic breakdown at the bottleneck in mixed traffic flow.

## I. INTRODUCTION

It is generally assumed that future vehicular traffic is a mixed traffic flow consisting of human driving and automated driving vehicles [1–16]. There exists a large series of papers by the well-known and massive "Automated Highway System" project involving the US government and a large number of transportation researchers in (especially) California [17,18], EU projects [19], and projects made in Germany [20]. A consortium of researchers all over the world performed extensive and pioneering research into connected vehicles and platooning interactions between such platoons and other vehicles (see references to this extensive research, for example, in reviews and books by Ioannou [1], Ioannou and Sun [2], Ioannou and Kosmatopoulos [3], Shladover [21], Rajamani [7], Meyer and Beiker [8], and Bengler *et al.* [9]).

Automated driving vehicles (called also autonomous driving, automatic driving, or self-driving vehicles) should considerably enhance highway capacity. Highway capacity is limited by traffic breakdown at road bottlenecks. Traffic breakdown is a transition from free flow at a bottleneck to congested traffic at the bottleneck [22–35]. Elefteriadou *et al.* have found [36] that empirical traffic breakdown at a highway bottleneck exhibits a probabilistic nature: At the same flow rate in free flow at a bottleneck traffic breakdown can occur but it should not necessarily occur. Empirical probability of traffic breakdown at highway bottlenecks found first by Persaud *et al.* [37] is a growing function of the flow rate in free flow. Because empirical traffic breakdown in free flow at a bottleneck is a probabilistic phenomenon, the probability of traffic breakdown in free flow at the bottleneck is one of the main characteristics of the traffic stream. Therefore, the main objective of this paper is to find the effect of different features of the dynamics of automated driving vehicles in a mixed traffic flow on the probability of traffic breakdown in free flow at a highway bottleneck.

As known (see, e.g., reviews and books [22–25,33–35] and references therein), the most important features of

traffic breakdown in free flow at an on-ramp bottleneck on a single-lane road are qualitatively the same as those in highly heterogeneous traffic flow consisting of very different types of vehicles on a multilane road with different types of road bottlenecks. In particular, this conclusion is related to the empirical flow-rate dependence of the breakdown probability [25,35]. Therefore, to find the effect of different features of the dynamics of automated driving vehicles in mixed traffic flow on the probability of traffic breakdown at a road bottleneck, it is sufficient to study a simple case of mixed vehicular traffic where traffic consists only of two types of vehicles (human driving and automated driving vehicles) moving on a single-lane road with an on-ramp bottleneck.

On the single-lane road, no vehicles can pass. For this reason, the physics of automated driving can be understood through an analysis of an adaptive cruise control (ACC) in a vehicle: An ACC vehicle follows the preceding vehicle (that can be either a human driving vehicle or an ACC vehicle) automatically based on some ACC dynamics rules of motion (see, e.g., [1–7,11–13,15,16]). In a classical ACC model, acceleration (deceleration) $a^{(\mathrm{ACC})}$ of the ACC vehicle is determined by the space gap to the preceding vehicle $g$ and the relative speed $\Delta v = v_\ell - v$ measured by the ACC vehicle as well as by a desired time headway $\tau_{\mathrm{d}}^{(\mathrm{ACC})}$ of the ACC vehicle to the preceding vehicle (see, e.g., [4–7,11–13,15,16] and references therein):

$$a^{(\mathrm{ACC})} = K_1\big(g - v\tau_{\mathrm{d}}^{(\mathrm{ACC})}\big) + K_2(v_\ell - v), \qquad (1)$$

where $v$ is the speed of the ACC vehicle, $v_\ell$ is the speed of the preceding vehicle; here and below $v$, $v_\ell$, and $g$ are time functions; $K_1$ and $K_2$ are coefficients of ACC adaptation. It is well known that there can be string instability of a long enough platoon of ACC vehicles (1) [4–7,11–13,15,16]. As found by Liang and Peng [5], the string instability occurs under condition $K_2 < [2 - K_1(\tau_{\mathrm{d}}^{(\mathrm{ACC})})^2]/2\tau_{\mathrm{d}}^{(\mathrm{ACC})}$. Coefficients $K_2$ and $K_1$ of classical ACC (1) can be chosen to satisfy conditions for string stability.

042303-1

It should be mentioned that the effect of classical ACC vehicles (1) on mixed traffic flow consisting of ACC vehicles and human driving vehicles was intensively considered already in 1990s and 2000s in the works by Dharba and Rajagopal [38], Marsden *et al.* [39], VanderWerf *et al.* [40,41], Treiber and Helbing [42], Li *et al.* [43], Kukuchi *et al.* [44], Bose and Ioannou [45], Suzuki [46], Davis [15], Zhou and Peng [47], van Arem *et al.* [48], Martinez and Canudas-do-Wit [49], Kesting *et al.* [50,51], and Lin *et al.* [52]; this is a subject of intensive studies (see, e.g., [16,53–59] and references therein).

From studies of empirical traffic data measured over years on different highways it has been found that traffic breakdown at a highway bottleneck is a phase transition from free flow (F) to synchronized flow (S); this F → S transition exhibits the nucleation nature [60,61]. This means that traffic breakdown occurs in a metastable free flow with respect to an F → S transition at the bottleneck. This metastability of free flow is as follows [60,61]: There can be many speed (density, flow rate) disturbances in free flow at the bottleneck. Amplitudes of the disturbances can be very different. When a disturbance occurs randomly whose amplitude is larger than a critical one, then traffic breakdown occurs. Such a disturbance resulting in the breakdown is called the *nucleus* for the breakdown. Otherwise, if the disturbance amplitude is smaller than the critical one, the disturbance decays; as a result, no traffic breakdown occurs. As proven in details in Refs. [33–35], classical traffic flow theories and models of human driving vehicles cannot explain the empirical nucleation nature of traffic breakdown (F → S transition) at the bottleneck. This critical conclusion is also related to models of human driving vehicles used for studies of mixed traffic flow in [38–59].

To explain the empirical nucleation nature of traffic breakdown (F → S transition) at the bottleneck, the author has introduced the three-phase traffic theory [60,62]. The three-phase theory is the framework for understanding of states of empirical traffic flow in three phases: (i) free flow, (ii) synchronized flow, and (iii) wide-moving jam; the synchronized flow and wide-moving jam phases belong to congested traffic (see, e.g., [33–35,64,65]). One of the first traffic flow models in the framework of the three-phase theory is the Kerner-Klenov microscopic stochastic model [66–68]. This traffic flow model can show the nucleation nature of traffic breakdown (F → S transition) at the bottleneck as observed in empirical data.

The effect of classical ACC vehicles (1) on traffic flow in which human driving vehicles have been simulated with the Kerner-Klenov model in the framework of the three-phase theory has been studied in [65]. It has been found that even if any platoon of classical ACC vehicles (1) is stable, it can occur that already a small share of classical ACC vehicles in mixed traffic flow can deteriorate traffic while provoking traffic breakdown at network bottlenecks [65].

In this article, we introduce a model of ACC in the framework of the three-phase theory (called TPACC; see explanations below). Based on the model of TPACC, we make a comparison of the effect of classical ACC vehicles and TPACC vehicles on the probability of traffic breakdown at a road bottleneck in mixed traffic flow. Because the Kerner-Klenov microscopic stochastic model [66–68] can show the nucleation nature of traffic breakdown (F → S transition) at the bottleneck as observed in empirical data, for all simulations of human
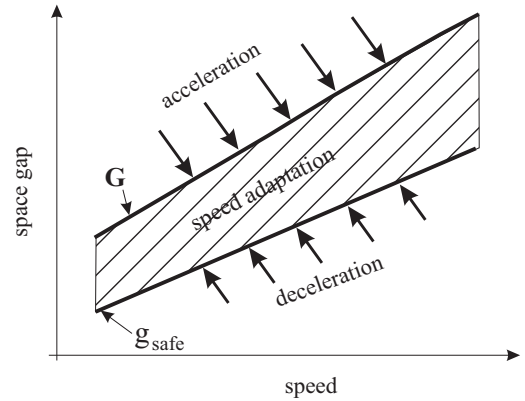


FIG. 1. Qualitative explanation of operating points of TPACC. Qualitative presentation of a part of 2D region for operating points of TPACC in the space gap–speed plane: At a given speed of TPACC vehicle there are the infinity of operating points of TPACC [69]. $G$ is a synchronization space gap, $g_{safe}$ is a safe space gap.

driving vehicles in mixed traffic flow we use the Kerner-Klenov traffic flow model.

To understand the idea of ACC in the framework of the three-phase theory, first it should be noted that in the works devoted to analysis of the effect of automated driving on traffic flow [38–59], traffic flow models for human driving vehicles have been used in which at a given time-independent vehicle speed there is a single model solution for a space gap to the preceding vehicle. Therefore, for hypothetical steady state model solutions, there is a one-dimensional (1D) relationship between a chosen speed and the related desired (or optimal) space gap to the preceding vehicle. This well-known assumption for traffic flow models of human driving vehicles used in [38–59] is qualitatively the same as the existence of a desired time headway $\tau_d^{(ACC)}$ of the ACC vehicle to the preceding vehicle: For the classical ACC rule (1) that satisfies conditions for string stability, at a given ACC speed $v$ there is a single operating point for a desired space gap $g^{(ACC)} = v\tau_d^{(ACC)}$.

However, a study of real field traffic data shows [60] that the existence of a desired time headway $\tau_d^{(ACC)}$ of the ACC vehicle to the preceding vehicle is inconsistent with a basic behavior of real drivers in car following: Empirical data show that real drivers do not try to reach a fixed time headway to the preceding vehicle in car following. To explain this empirical fact, in the three-phase theory it is assumed that when a driver approaches a slower moving preceding vehicle and the driver cannot pass it, the driver decelerates within a synchronization space gap $G$. This speed adaptation to the speed of the preceding vehicle occurs without caring what the precise space gap $g$ to the preceding vehicle is as long as it is not smaller than a safe space gap $g_{safe}$ [60]. The speed adaptation occurring within the synchronization space gap $G$ leads to a 2D region of traffic flow states (dashed region in Fig. 1 that can also be considered as the "indifference zone" in car following) determined by conditions

$$g_{safe} \leqslant g \leqslant G. \qquad (2)$$

In other words, accordingly to (2), drivers do not try to reach a particular (desired or optimal) time headway to the preceding

vehicle, but adapt the speed while keeping time headway $\tau^{(net)} = g/v$ in a range $\tau_{safe} \leqslant \tau^{(net)} \leqslant \tau_G$, where $\tau_G = G/v$, $\tau_G$ is a synchronization time headway, $\tau_{safe} = g_{safe}/v$ is a safe time headway, and it is assumed that the speed $v > 0$.

We define "automated driving in the framework of three-phase traffic theory" as follows:

Automated driving in the framework of the three-phase traffic theory is an automated driving for which there is *no* fixed time headway to the preceding vehicle.

A relation of this definition to real automated driving vehicles will be discussed in Sec. VII A.

In inventions [69], we have assumed that to satisfy these empirical features of real traffic, acceleration (deceleration) of automated driving in the framework of the three-phase theory (for short, Three-traffic-Phase ACC: TPACC) [70] should be given by the formula [69]

$$a^{(TPACC)} = K_{\Delta v}(v_\ell - v) \quad \text{at} \quad g_{safe} \leqslant g \leqslant G, \quad (3)$$

where $K_{\Delta v}$ is a dynamic coefficient ($K_{\Delta v} > 0$).

The hypothesis about the 2D region of traffic flow (indifference zones in car following; dashed region in Fig. 1) introduced in the three-phase theory [60], car-following models for human driving vehicles with indifference zones in car followingquery, [66–68,71] first developed in [66], and the concept of TPACC strategy (3) [69] are known. However, there is no TPACC model that is suitable for studies of physical characteristics of TPACC in mixed traffic flow. Therefore, the physics of TPACC has not been known up to now. In this paper, we disclose the physical characteristics of TPACC vehicles and the physics of the effect of TPACC vehicles on traffic flow.

The main contributions of this paper are as follows:

(i) We introduce a simple TPACC model that allows us to simulate physical features of mixed traffic flow consisting of human driving vehicles and TPACC vehicles.

(ii) We will show that the mean amplitude of speed disturbances at a road bottleneck occurring through TPACC vehicles can be considerably smaller than introduced by classical ACC vehicles at the same model parameters.

(iii) We will show that in mixed traffic flow with TPACC vehicles the probability of traffic breakdown at a road bottleneck can be considerably smaller than in mixed traffic flow with classical ACC vehicles.

(iv) We disclose the physics of the improving of the traffic stream through TPACC vehicles mentioned in item (iii).

The article is organized as follows: In Sec. II, we introduce a simple TPACC model that allows us to study the physics of automated driving in the framework of the three-phase theory. Simulations of string stability of ACC vehicles and TPACC vehicles at an on-ramp bottleneck are made in Sec. III. Speed disturbances that occur by passing of ACC vehicles and TPACC vehicles through the on-ramp bottleneck are the subject of Sec. IV. An analysis of the probability of traffic breakdown at the bottleneck in mixed traffic flow is presented in Sec. V. Traffic stream flow characteristics of mixed traffic flow are discussed in Sec. VI. In Sec. VII, we consider the applicability of the TPACC model for a reliable analysis of some features of future automated driving in mixed traffic flow (Sec. VII A) and formulate the paper's conclusions (Sec. VII B). In appendices, we present the Kerner-Klenov stochastic microscopic three-phase model for human driving

vehicles [66–68] used for simulations of mixed traffic flow (Appendix A), explain simulations of the classical ACC model (1) (Appendix B), and consider the model of vehicle merging at an on-ramp bottleneck (Appendix C).

## II. MODEL OF ACC IN FRAMEWORK OF THREE-PHASE THEORY (TPACC)

### A. Main equations

We introduce the following TPACC model:

$$a^{(TPACC)} = \begin{cases} K_{\Delta v}(v_\ell - v) & \text{at} \quad g \leqslant G, \\ K_1(g - v\tau_p) + K_2(v_\ell - v) & \text{at} \quad g > G, \end{cases} \quad (4)$$

where $\tau_p$ is a model parameter and it is assumed that $g \geqslant g_{safe}$. In comparison with the TPACC strategy (3), the TPACC model (4) allows us to simulate physical features of TPACC vehicles in mixed traffic flow.

### B. Discrete version of TPACC model

Simulations of human driving vehicles in mixed traffic flow are made with the car-following model in the framework of the three-phase theory [66,67] with discrete time $t = n\tau$, where $n = 0, 1, 2, \ldots$; $\tau = 1$ s is time step. The models of human driving vehicles [66,67] are continuous in space. We use a version of this model [68] that is discrete in space: A very small value of the discretization space interval $\delta x = 0.01$ m is used in the model. As explained in [68], this allows us to make more accurate simulations of traffic breakdown at road bottlenecks [71]. Because the model for human driving vehicles [66–68] is discrete in time, we simulate the TPACC model (4) with discrete time $t = n\tau$. Because models of mixed traffic flow consisting of human driving vehicles and the classical ACC have been considered in [65], these models have been given in the appendices.

Respectively, TPACC model (4) should be rewritten as follows:

$$a_n^{(TPACC)} = \begin{cases} K_{\Delta v}(v_{\ell,n} - v_n) & \text{at} \quad g_n \leqslant G_n, \\ K_1(g_n - v_n\tau_p) + K_2(v_{\ell,n} - v_n) & \text{at} \quad g_n > G_n, \end{cases}$$
$$(5)$$

where $G_n = v_n\tau_G$.

#### 1. Safety conditions

When $g_n < g_{safe,n}$, the TPACC vehicle should move in accordance with some safety conditions to avoid collisions between vehicles (Fig. 1). A collision-free TPACC vehicle motion is described as made in [65] for the classical model of ACC:

$$v_{c,n}^{(TPACC)} = v_n + \tau \max\left(-b_{max}, \min\left(\lfloor a_n^{(TPACC)} \rfloor, a_{max}\right)\right), \quad (6)$$

$$v_{n+1} = \max\left(0, \min\left(v_{free}, v_{c,n}^{(TPACC)}, v_{s,n}\right)\right), \quad (7)$$

where the TPACC acceleration and deceleration are limited by $a_{max}$ and $b_{max}$, respectively; the speed $v_{n+1}$ (7) at time step $n+1$ is limited by the maximum speed $v_{free}$ and by the safe speed $v_{s,n}$ that have been chosen, respectively, the same as those in the model of human driving vehicles; $\lfloor z \rfloor$ denotes the integer part of $z$ [128] (see Appendix A).
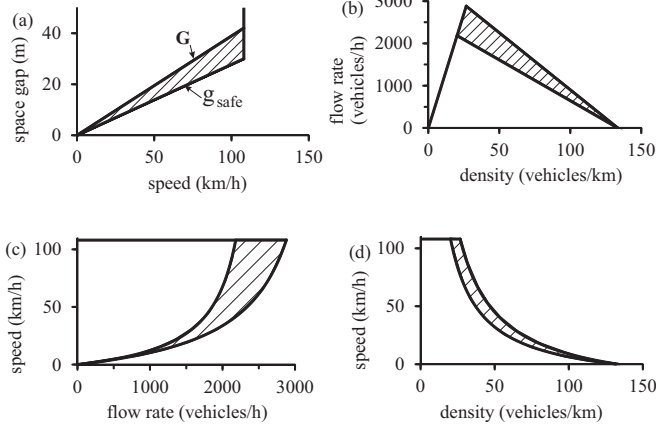
FIG. 2. Operating points of TPACC model (5)–(7) presented in the space gap–speed (a), flow-density (b), speed-flow (c), and speed-density (d) planes. Model parameters $\tau_G = 1.4$ s, $\tau_p = 1.3$ s, $\tau_{safe} = 1$ s, $v_{free} = 30$ m/s (108 km/h), vehicle length (including the mean space gap between vehicles stopped within a wide moving jam) $d = 7.5$ m.

#### 2. "Indifference zone" in car following

In accordance with Eq. (7), condition $v_{c,n}^{(TPACC)} \leqslant v_{s,n}$ is equivalent to condition $g_n \geqslant g_{safe,n}$. Under this condition, from the TPACC model (5)–(7) it follows that when time headway $\tau_n^{(net)} = g_n/v_n$ of the TPACC vehicle to the preceding vehicle is within the range

$$\tau_{safe,n} \leqslant \tau_n^{(net)} \leqslant \tau_G, \qquad (8)$$

the acceleration (deceleration) of the TPACC vehicle does not depend on time headway. In (8), $\tau_{safe,n} = g_{safe,n}/v_n$ is a safe time headway and it is assumed that $v_n > 0$.

In accordance with (8), for the TPACC model (5)–(7) there is *no* fixed desired time headway to the preceding vehicle (Fig. 1). This means that in the TPACC model (5)–(7) there is "indifference zone" in the choice of time headway in car following. This is in contrast with the classical ACC model (1) for which there is a fixed desired time headway in car following.

#### 3. Operating points

From the formula for the safe speed $v_{s,n}$ in (7) that is given in Appendix A 7, we find that the safe time headway $\tau_{safe,n}$ in (8) for the operating points of the TPACC model (5)–(7) is a constant value that is equal to $\tau_{safe} = 1$ s; therefore, the safe space gap $g_{safe} = v\tau_{safe}$. In operating points of the TPACC model (5)–(7), $a^{(TPACC)} = 0$; respectively, $v = v_\ell$, $g_{safe}(v) \leqslant g \leqslant G(v)$, and $v = v_{free}$ at $g > G(v)$, where $g_{safe}(v) = v\tau_{safe}$, $G(v) = v\tau_G$. The operating points of the TPACC model (5)–(7) cover a 2D region in the space gap–speed plane [dashed 2D region in Fig. 2(a)]. The inequalities $v \leqslant v_{free}$, $g \leqslant G(v)$, and $g \geqslant g_{safe}(v)$ define a 2D region in the space gap–speed plane [Fig. 2(a)] in which the operating points exist for the discrete version of the TPACC model (5)–(7) [125].

From Fig. 2, we can see that under conditions $g_{safe}(v) \leqslant g \leqslant G(v)$ for each given speed $v > 0$ of TPACC there is no fixed time headway to the preceding vehicle in operating points of the TPACC model (dashed 2D regions in Fig. 2), as explained in Sec. I (Fig. 1).
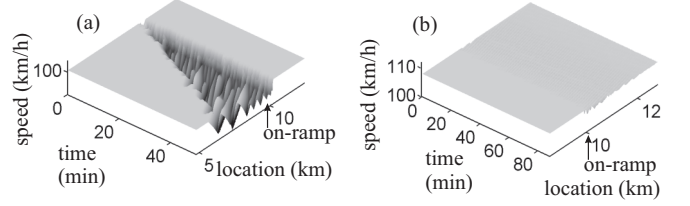


FIG. 3. Simulations of string instability of the classical ACC model (1) (see Appendix B) (a) and string stability of TPACC model (5)–(7) (b) in traffic flow consisting of 100% of automated driving vehicles on a single-lane road with on-ramp bottleneck located at $x_{on} = 10$ km (see Appendix C); speed in space and time. Simulation parameters of ACC (a) and TPACC (b) are identical ones: the on-ramp inflow rate $q_{on} = 320$ vehicles/h and the flow rate upstream of the bottleneck $q_{in} = 2002.6$ vehicles/h, $\tau_d^{(ACC)} = \tau_p = 1.3$ s, $\tau_G = 1.4$ s, $K_1 = 0.3$ s$^{-2}$, and $K_2 = K_{\Delta v} = 0.3$ s$^{-1}$; $a_{max} = b_{max} = 3$ m/s$^2$, $v_{free} = 30$ m/s (108 km/h), vehicle length $d = 7.5$ m. In accordance with the desired time headway $\tau_d^{(ACC)} = 1.3$ s of the ACC vehicles, the sum flow rate $q_{sum} = q_{in} + q_{on} = 2322.6$ vehicles/h is related to time headway 1.3 s between vehicles in free flow.

### III. SIMULATIONS OF STRING STABILITY OF ACC AND TPACC VEHICLES AT ON-RAMP BOTTLENECK

Simulations of string instability of ACC vehicles are shown in Fig. 3(a). Speed disturbances in traffic flow consisting of 100% ACC vehicles occur at an on-ramp bottleneck at which the on-ramp inflow with the rate $q_{on}$ and upstream flow with the rate $q_{in}$ merge. String instability of ACC vehicles leads to the emergence of moving jams upstream of the bottleneck [Fig. 3(a)].

Contrarily, at the same set of the flow rates $q_{on}$ and $q_{in}$ as well as the same other model parameters *no* string instability of any platoon of the TPACC vehicles is realized: In Fig. 3(b), all speed disturbances occurring at the bottleneck decay upstream of the bottleneck. It turns out that as long as time headway between TPACC vehicles is within the range (8), speed disturbances decay over time. This is because within this range the acceleration (deceleration) of TPACC vehicles does not depend on time headway to the preceding vehicle.

### IV. SPEED DISTURBANCES OCCURRING BY PASSING OF ACC AND TPACC VEHICLES THROUGH ON-RAMP BOTTLENECK

At a larger value of $K_2$ in (1) as well as at the same desired time headway $\tau_d^{(ACC)} = 1.3$ s and the same set of the flow rates $q_{on}$ and $q_{in}$ as those in Fig. 3, platoons of ACC vehicles become stable [Fig. 4(a)].

However, it turns out that considerable local speed disturbances appear at the bottleneck. This case is shown in Figs. 4(b), 4(c) in which ACC vehicle 2 merges from the on-ramp onto the main road following ACC vehicle 1 moving on the main road. To satisfy the desired time headway $\tau_d^{(ACC)}$, ACC vehicle 2 should decelerate to a lower speed than the minimum speed of ACC vehicle 1. This deceleration of ACC vehicle 2 forces the following ACC vehicle 3 to decelerate while approaching ACC vehicle 2. Simulations show that the occurrence of large local speed disturbances at the bottleneck
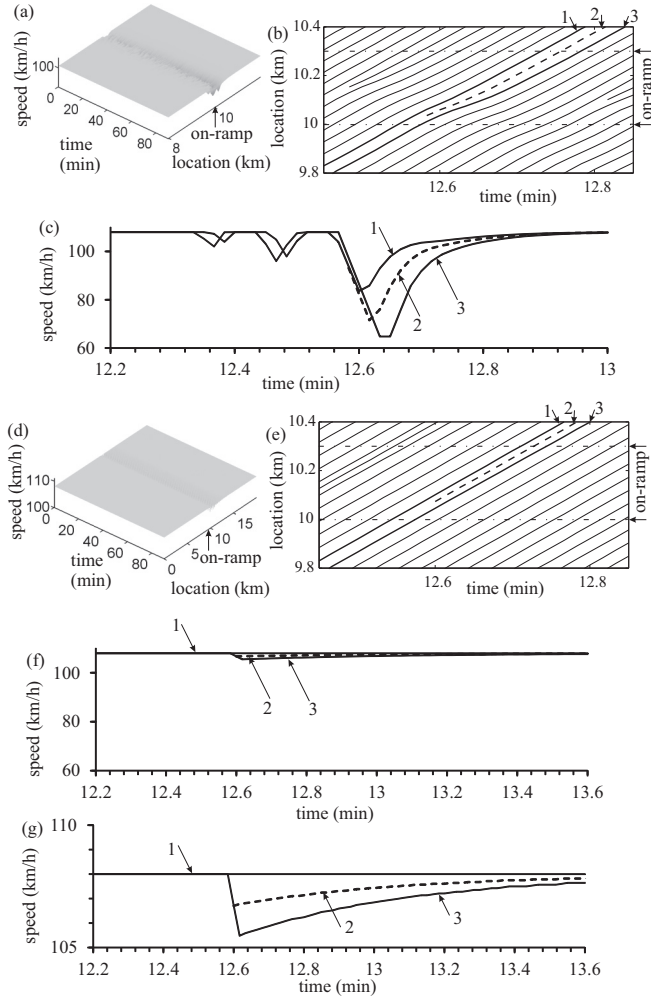
FIG. 4. Speed disturbances at on-ramp bottleneck in stable free flow with 100% automated driving vehicles for classical ACC model (1) (see Appendix B) [(a)–(c)] and for TPACC model (5)–(7) [(d)–(g)]: (a), (d) Speed in space and time. (b), (e) Fragments of vehicle trajectories; (b) is related to (a) and (e) is related to (d). (c), (f), (g) Microscopic speeds along vehicle trajectories shown by, respectively, the same numbers as in (b), (e); (c) is related to (b); (f), (g) are related to (e); (f) and (g) show the same speed in different speed scales. Simulation parameters of ACC [(a)–(c)] and TPACC [(d)–(g)] are identical ones. $K_2 = K_{\Delta v} = 0.6$ s$^{-1}$. In (b, e), the on-ramp merging region that is within road locations $x_{on} \leqslant x \leqslant x_{on}^{(e)}$ (see Appendix C) is labeled by "on-ramp". Other model parameters are the same as those in Fig. 3.

is a basic problem of ACC vehicles based on the classical ACC strategy (1) in which ACC vehicles try to reach a desired time headway $\tau_d^{(ACC)}$.

These large local speed disturbances at the bottleneck caused by ACC vehicles [Figs. 4(b), 4(c)] do not occur in traffic flow consisting of TPACC vehicles [Figs. 4(d)–4(g)]. This is because within the range of time headway (8) the acceleration (deceleration) of a TPACC vehicle does not depend on time headway. This explains small amplitudes of local speed disturbances caused by TPACC vehicles 2 and 3 at the bottleneck [Figs. 4(e)–4(g)]. The local speed disturbances caused by TPACC vehicles are so small [Fig. 4(f)] that on the same speed

scale as that used for the classical ACC [Fig. 4(c)] they almost cannot be resolved. Only at considerably larger speed scales do the local speed disturbances become visible [Fig. 4(g)].

## V. PROBABILITY OF TRAFFIC BREAKDOWN AT BOTTLENECK IN MIXED TRAFFIC FLOW

As mentioned in Sec. I, traffic breakdown in traffic flow of human driving vehicles is an F → S transition. Traffic breakdown occurs in a metastable free flow with respect to the F → S transition. Local speed disturbances caused by vehicle interactions in a neighborhood of the bottleneck can randomly initiate traffic breakdown in the metastable free flow. Such traffic breakdown has been called *spontaneous* traffic breakdown (spontaneous F → S transition). The larger the amplitude of local speed disturbances at the bottleneck, the more probable the nucleus occurrence for the spontaneous breakdown; i.e., the larger the probability of traffic breakdown $P^{(B)}$ at the bottleneck [33–35,60,65,126,127].

In the near future, we could expect mixed traffic flow in which the share of automated driving vehicles is small (Figs. 5 and 6). Single TPACC vehicles moving in such mixed traffic flow cause very small speed disturbances at the bottleneck [Figs. 6(a)–6(c)]. Indeed, we have found that the probability of traffic breakdown remains in this mixed flow the same as that in traffic flow consisting of human drivers only (curve 1 in Fig. 5). Contrarily, the probability of traffic breakdown can increase even when a very small number of classical ACC vehicles are in mixed traffic flow (curves 2 and 3 in Fig. 5). This deterioration of traffic through classical automated driving is explained by
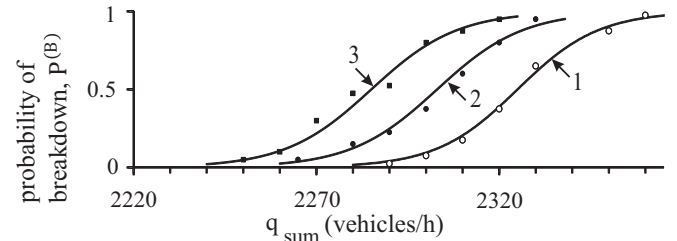


FIG. 5. Effect of small share of automated driving vehicles in mixed traffic flow on the flow-rate function of the probability $P^{(B)}(q_{sum})$ of traffic breakdown at on-ramp bottleneck on single-lane road, where $q_{sum} = q_{in} + q_{on}$. $P^{(B)}(q_{sum})$ is calculated through the change in the on-ramp inflow rate $q_{on}$ at a given flow rate $q_{in} = 2000$ vehicles/h. Curve 1 is related to traffic flow without automated driving vehicles as well as to mixed traffic flow with 2% of TPACC vehicles. Curves 2 and 3 are related to mixed traffic flow with 2% of ACC vehicles, respectively, with $\tau_d^{(ACC)} = 1.3$ s (curve 2) and 1.6 s (curve 3). Other model parameters for ACC vehicles and TPACC vehicles are, respectively, the same as those in Fig. 4. For calculation of $P^{(B)}(q_{sum})$, at each given value $q_{sum}$ different simulation realizations (runs) $N_r = 40$ during the same time interval for the observing of traffic flow $T_{ob} = 30$ min have been made. The different realizations have been performed at the same set of model parameters, however, at different values of the initial values of random function rand( ) in the traffic flow model (see Appendices A 4 and A 5). Then, $P^{(B)}(q_{sum}) = n_r/N_r$, where $n_r$ is the number of realizations in which traffic breakdown has occurred during the time interval $T_{ob}$ (a more detailed explanation of calculation of the function $P^{(B)}(q_{sum})$ has been given in Ref. [35]).
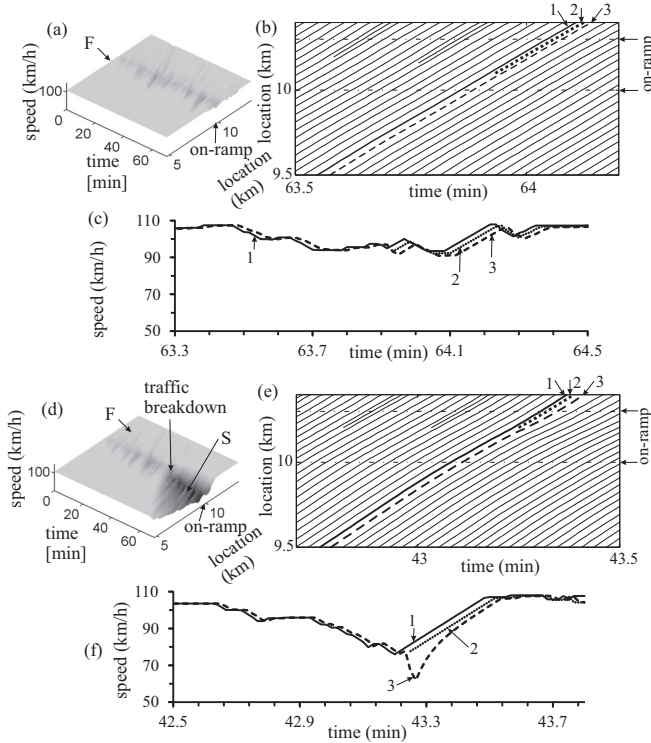
FIG. 6. Explanation of the effect of a single automated driving vehicle on the probability of traffic breakdown at on-ramp bottleneck in mixed traffic flow associated with Fig. 5; speed disturbances occurring at on-ramp bottleneck through a single TPACC vehicle [(a)–(c)] and a single ACC vehicle [(d)–(f)]: (a), (d) Speed in space and time. (b), (e) Fragments of vehicle trajectories. (c), (f) Microscopic speeds along vehicle trajectories shown by the same numbers in (b), (e), respectively. In (b), (c), (e), (f), vehicles 1 and 2 are human driving vehicles whereas vehicle 3 is TPACC vehicle in (b), (c) and ACC vehicle in (e), (f). Mixed traffic flow with 2% of automated driving vehicles; $q_{in} = 2000$ vehicles/h, $q_{on} = 280$ vehicles/h; other model parameters for ACC vehicles and TPACC vehicles are, respectively, the same as those in Fig. 4. In (a), (d): F, free flow; S, synchronized flow.

the occurrence of a large amplitude speed disturbance caused by a classical ACC vehicle at the bottleneck [Figs. 6(d)–6(f)]: Already a single ACC vehicle can initiate traffic breakdown at the bottleneck [Figs. 6(d)–6(f)].

If the share of automated driving vehicles in mixed traffic flow increases (Fig. 7), the probability of traffic breakdown caused by ACC vehicles that deteriorate traffic can increase considerably (curve 3 in Fig. 7). Contrarily, long enough platoons of TPACC vehicles in mixed traffic flow decrease the breakdown probability (curve 2 in Fig. 7).

This physical feature of TPACC vehicles is also explained by the speed adaptation effect of the three-phase theory that is the basis of TPACC (4): At each vehicle speed, the TPACC vehicle makes an arbitrary choice in time headway that satisfies conditions (8). In other words, the TPACC vehicle accepts different values of time headway at different times and does not control a fixed time headway to the preceding vehicle. This dynamic behavior of TPACC vehicles decreases the amplitude of local speed disturbances at the bottleneck [Figs. 4(d)–4(g)]. This explains why, in contrast to classical ACC vehicles,
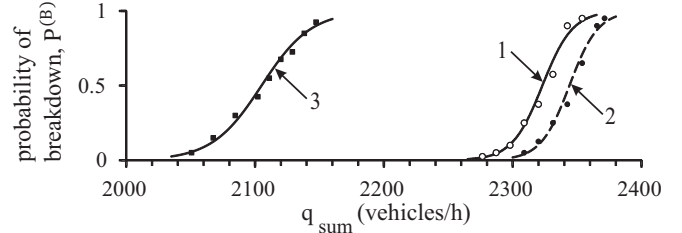


FIG. 7. Probability of traffic breakdown at on-ramp bottleneck as a function of the flow rate $q_{sum} = q_{in} + q_{on}$ at a given on-ramp inflow rate $q_{on} = 320$ vehicles/h in mixed traffic flow with 20% automated driving vehicles: Curve 1 is related to traffic flow without automated driving vehicles. Curves 2 and 3 are related to mixed traffic flow with TPACC vehicles (curve 2) and ACC vehicles (curve 3). Simulation parameters of ACC and TPACC are, respectively, the same as those in Fig. 4.

TPACC vehicles decrease the probability of traffic breakdown in mixed traffic flow.

## VI. TRAFFIC STREAM CHARACTERISTICS OF MIXED TRAFFIC FLOW

We can assume that vehicles implementing TPACC strategy (4) can reduce the overall flow for the traffic stream due to their different use of available space on the road. However, simulations presented in Figs. 3–7 show that no such adverse effect for the traffic stream occurs. To answer a question of how exactly flow is affected when the TPACC strategy versus the ACC strategy is considered, in this section we make a study of traffic stream flow characteristics related to simulations of mixed traffic flow presented in Figs. 4–7.

### A. Traffic stream flow characteristics of mixed traffic flow with 2% automated driving vehicles

In Fig. 8(a), we show the fundamental diagram (flow-density relationship) for free flow without automated driving vehicles. It turns out that these traffic stream flow characteristics are identical for traffic without automated driving vehicles and for mixed traffic with 2% of TPACC vehicles: Single TPACC vehicles do not affect the stream flow characteristics in free flow [Figs. 8(a), 8(b)]. This result has already been mentioned in Sec. V, when we have discussed curve 1 shown in Fig. 5 for the flow-rate dependence of the probability of traffic breakdown $P^{(B)}(q_{sum})$.

In the three-phase theory (see Refs. [33–35]), there is a deep connection between the flow-rate dependence of the probability of traffic breakdown $P^{(B)}(q_{sum})$ (Fig. 5) and the overall flow as well as other traffic stream flow characteristics [Figs. 8(c), 8(d)]. In particular, on traffic stream flow characteristics (such as flow-density and speed-flow relationships) one should distinguish a flow-rate range [Figs. 8(c), 8(d)]:

$$q_{th}^{(B)} \leqslant q_{sum} \leqslant C_{max}. \tag{9}$$

Within the flow-rate range (9), free flow is in a metastable state with respect to traffic breakdown (F $\rightarrow$ S transition) at the bottleneck. A characteristic flow rate $q_{sum} = q_{th}^{(B)}$ in (9) has been called a threshold flow rate for spontaneous traffic
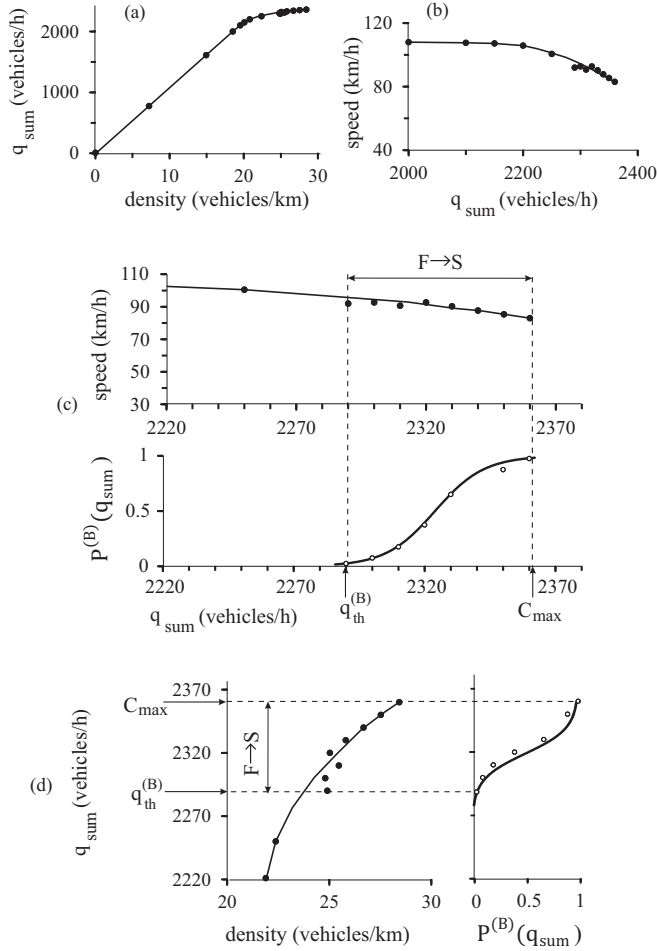
FIG. 8. Traffic stream flow characteristics for free flow on single-lane road with on-ramp bottleneck in traffic without automated driving vehicles and in mixed traffic with 2% of TPACC vehicles: (a) Flow-density relationship (fundamental diagram). (b) A part of speed-flow relationship for larger flow rates. (c), (d) Parts of speed-flow (c) and flow-density (d) relationships for larger flow rates versus the breakdown probability $P^{(B)}(q_{sum})$; function $P^{(B)}(q_{sum})$ is curve 1 from Fig. 5. To compare stream flow characteristics with simulations shown in Figs. 5 and 6, at $q_{sum} \leqslant 2000$ vehicles/h there is no on-ramp inflow ($q_{on} = 0$); at $q_{sum} = q_{in} + q_{on} > 2000$ vehicles/h, the increase in $q_{sum}$ has been achieved through increase in $q_{on}$ at constant $q_{in} = 2000$ vehicles/h. Traffic stream flow characteristics have been calculated as follows. At each given flow rate $q_{sum}$ (black points on the characteristics), 5-min averaged data for the speed, density, and flow rate have been measured with the use of a virtual road detector installed at the end of the on-ramp merging region $x = 10.3$ km. The data have been measured *only* during time interval within which free flow has been observed in a simulation realization. Then, as by the calculation of $P^{(B)}(q_{sum})$ in Fig. 5, $N_r = 40$ different realizations have been simulated for each of the chosen flow rates $q_{sum}$ (see caption to Fig. 5). This allows us to make a statistical analysis of the average speed and density in the traffic stream. Black points on the speed-flow and flow-density relationships are related to the average values of the speed and density derived from this statistical analysis. Other model parameters are the same as those in Fig. 4. Calculated values: $q^{(B)}_{th, TPACC} = q^{(B)}_{th} = 2290$ and $C_{max, TPACC} = C_{max} = 2360$ vehicles/h.
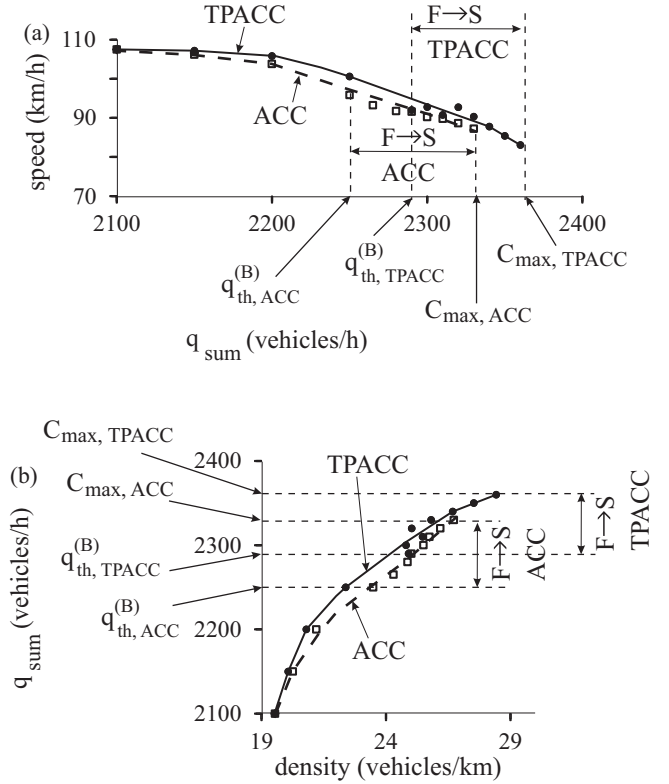


FIG. 9. Comparison of traffic stream flow characteristics for free flow on single-lane road with on-ramp bottleneck in mixed traffic with 2% of automated driving vehicles. Parts of flow-density (a) and speed-flow (b) relationships for larger flow rates. Solid curves "TPACC" are related to TPACC vehicles. Dashed curves "ACC" are related to classical ACC vehicles. Stream flow characteristics have been calculated as explained in caption to Fig. 8. Other model parameters are the same as those in Fig. 4. Calculated values: $q^{(B)}_{th, TPACC} = 2290$ and $C_{max, TPACC} = 2360$ vehicles/h; $q^{(B)}_{th, ACC} = 2265$ and $C_{max, ACC} = 2330$ vehicles/h.

breakdown at the bottleneck: At $q_{sum} < q^{(B)}_{th}$ the breakdown probability $P^{(B)} = 0$; i.e., no spontaneous traffic breakdown can occur during a time interval of the observation of traffic flow $T_{ob}$ (see caption to Fig. 5). A characteristic flow rate $q_{sum} = C_{max}$ in (9) has been called a maximum highway capacity: At $q_{sum} \geqslant C_{max}$ the breakdown probability $P^{(B)} = 1$; i.e., spontaneous traffic breakdown does occur at the bottleneck during the time interval $T_{ob}$.

The larger the values $q^{(B)}_{th}$ and $C_{max}$ for the traffic stream, the larger is on average the overall flow. Therefore, the characteristic flow rates $q^{(B)}_{th}$ and $C_{max}$, which determine the boundaries of the flow-rate range (9), are basic statistical characteristics of the overall flow in the traffic stream in the framework of the three-phase theory [129]. For the further analysis, we denote the flow-rate range (9) on traffic stream characteristics by the arrow "F → S" [Figs. 8(c), 8(d), 9, and 10].

At 2% of automated driving vehicles, the effect on the overall flow due to different use of space on the road by TPACC and ACC vehicles can be considered negligibly small. We denote the statistical characteristics of the overall flow $q^{(B)}_{th}$, $C_{max}$ in (9) for mixed traffic flow by $q^{(B)}_{th, TPACC}$, $C_{max, TPACC}$,
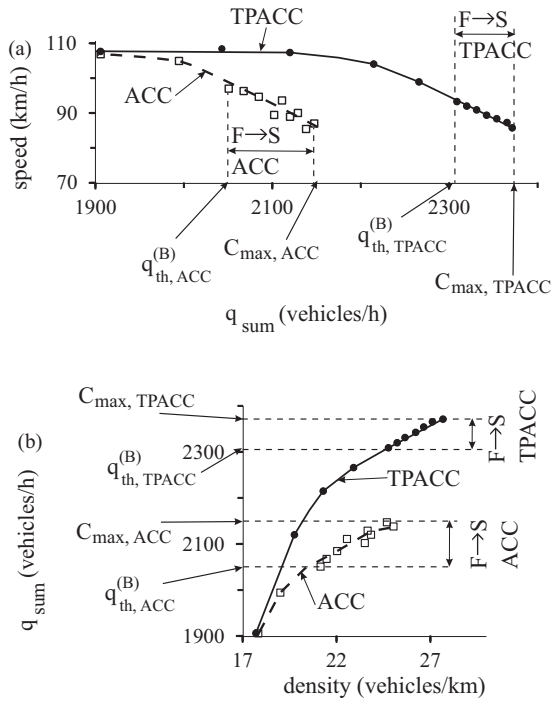
FIG. 10. Comparison of traffic stream flow characteristics for free flow on single-lane road with on-ramp bottleneck in mixed traffic with 20% of automated driving vehicles. Parts of flow-density (a) and speed-flow (b) relationships for larger flow rates. Solid curve "TPACC" is related to TPACC vehicles. Dashed curve "ACC" is related to classical ACC vehicles. Stream flow characteristics have been calculated as explained in caption to Fig. 8. Other model parameters are the same as those in Fig. 4. Calculated values: $q_{\mathrm{th,\,TPACC}}^{(B)} = 2308$ and $C_{\mathrm{max,\,TPACC}} = 2371$ vehicles/h; $q_{\mathrm{th,\,ACC}}^{(B)} = 2050$ and $C_{\mathrm{max,\,ACC}} = 2147$ vehicles/h.

when automated driving vehicles are TPACC vehicles, and by $q_{\mathrm{th,\,ACC}}^{(B)}$, $C_{\mathrm{max,\,ACC}}$ for classical ACC vehicles, respectively. We have found that the overall flow characteristics do not change on average in mixed traffic with 2% of TPACC vehicles (Fig. 8): $q_{\mathrm{th,\,TPACC}}^{(B)} = q_{\mathrm{th}}^{(B)}$ and $C_{\mathrm{max,\,TPACC}} = C_{\mathrm{max}}$.

In contrast with mixed traffic flow with 2% of TPACC vehicles, we have found that both values $q_{\mathrm{th,\,ACC}}^{(B)}$ and $C_{\mathrm{max,\,ACC}}$ decrease in mixed traffic flow with 2% of classical ACC vehicles (Fig. 9, curve "ACC"). This means that already 2% of classical ACC vehicles reduce on average the overall flow in the traffic stream. As explained in Secs. IV and V, this result is associated with a large local speed disturbance caused by a classical ACC vehicle at the bottleneck: Within the flow-rate range (9), the large local speed disturbance can initiate a nucleus for spontaneous traffic breakdown at the bottleneck.

### B. Traffic stream flow characteristics of mixed traffic flow with 20% automated driving vehicles

At 20% of automated driving vehicles in mixed traffic flow, we can expect that there should be the effect of different use of available space on the road through the different dynamic behavior of TPACC vehicles and ACC vehicles on the overall flow in the traffic stream. However, rather than reduction of the overall flow through the use of TPACC vehicles, we have

found that TPACC vehicles increase on average the overall flow (compare values $q_{\mathrm{th,\,TPACC}}^{(B)}$, $C_{\mathrm{max,\,TPACC}}$ in Fig. 8 with, respectively, these values given in the caption to Fig. 10).

In contrast with TPACC vehicles, we have found that classical ACC vehicles reduce on average the overall flow in mixed traffic flow (Fig. 10). As explained in Secs. IV and V, this effect of the overall flow reduction caused by classical ACC vehicles is explained by the occurrence of large local speed disturbances at the bottleneck in mixed traffic flow. The local speed disturbances initiate traffic breakdown in the mixed traffic flow at considerably smaller flow rates in comparison with traffic flow without classical ACC vehicles. Thus, through the strong effect of automated driving vehicles on traffic breakdown at the bottleneck, in simulations we cannot resolve the effect of the different use of available space on the road by TPACC vehicles and ACC vehicles on the overall flow [130].

We have found that automated driving based on the TPACC strategy can increase on average the overall flow for mixed traffic flow; contrarily, automated driving based on the classical ACC strategy decreases on average the overall flow (Figs. 9 and 10). We can expect that other objectives of a comparison of the TPACC strategy versus the ACC strategy can be interesting for further studies that are out of the scope of this paper. Examples are a study of (i) congested mixed traffic build at the bottleneck after traffic breakdown has occurred or (ii) characteristics of mixed traffic flow consisting of automated driving and human driving vehicles with different driver and vehicle parameters, or else (iii) the effect of the TPACC strategy on multilane mixed traffic with different types of bottlenecks.

## VII. DISCUSSION

### A. About applicability of model results for future automated driving in mixed traffic flow

There have been no TPACC models related to the TPACC strategy [69] that could be used for an analysis of TPACC vehicles in different driving situations. Therefore, the effect of TPACC vehicles on traffic flow could not be studied before. We have shown that a TPACC model (4) introduced in this paper has allowed us to understand the physics of TPACC vehicles in mixed traffic flow. In particular, we have found the effect of TPACC vehicles on the probability of traffic breakdown at a road bottleneck. However, the following question can arise: Can the simple TPACC model (4) be applicable for reliable statements about physical features of real mixed traffic flow consisting of human driving vehicles and TPACC vehicles? To answer this question, we consider first some features of the TPACC model (4) that might appear at first glance nonrealistic for real traffic flow.

It seems that TPACC model (4) is mathematically of small incremental value from the pre-existing classical ACC model (1). However, in the paper we have shown that this "small incremental mathematical value" exhibits a large physical effect on traffic flow. This large physical effect on traffic flow through the TPACC strategy (4) is associated with the TPACC physical feature mentioned above: Through the indifference zone of TPACC (4), a TPACC vehicle does not react on the time headway change within the time headway range (8). This dynamic behavior of TPACC vehicles decreases local speed

disturbances in free flow at the bottleneck. The reduction of the local speed disturbances results in a decrease in the breakdown probability in the traffic stream.

Another question can arise from the choice of the model time step $\tau = 1$ s in Eqs. (5)–(7) that have been used for numerical simulations of TPACC model (4): In TPACC model (5)–(7), the time step $\tau = 1$ s determines the safe space gap $g_{\rm safe} = v\tau$ under hypothetical steady state conditions in which all vehicles move at time-independent speed $v$. Contrarily to the TPACC model (5)–(7), typical ACC controllers in vehicles that on the market have update time intervals $\tau$ of 100 ms or less. Indeed, there may be some very dangerous traffic situations in real traffic in which the safe time headway for an ACC vehicle is quickly reached and, therefore, the ACC vehicle must decelerate strongly already after a time interval that is a much shorter than 1 s to avoid the collision with the preceding vehicle. Therefore, to avoid collisions, *real* ACC controllers must have update time intervals $\tau$ of 100 ms or less. However, at model time step $\tau = 1$ s through the choice in the mathematical formulation of the safe speed in TPACC model (5)–(7) and in the model of human driving vehicles (see Appendices A 7 and B), *collisionless* traffic flow is guaranteed in *any* dangerous traffic situation that can occur in simulations of traffic flow.

In other words, to disclose the physics of TPACC the choice of the update time $\tau = 1$ s is sufficient in *simulations* of TPACC behavior. To explain this, we should note that Eqs. (6), (7) affect TPACC dynamics *only* under condition $g_n \leqslant g_{\rm safe,n}$, i.e., when the space gap becomes smaller than the safe one. This is because the physics of TPACC disclosed in this paper is *solely* determined by Eq. (5): Under condition $g_n \geqslant g_{\rm safe,n}$, Eqs. (6), (7) do not change TPACC acceleration (deceleration) calculated through Eq. (5).

This paper deals with a subset of the functionality required for automated driving, namely longitudinal following a given leader (TPACC). Other challenges for automated driving such as lateral dynamics or sensor-related problems, which are important to satisfy a safety motion of automated driving vehicles on multilane highways and urban areas (see, e.g., [1–3,7–10]), are not tackled in this paper. Therefore, a question can arise as to what degree results derived for TPACC are related to future automated driving.

As mentioned in Sec. I, in empirical data the qualitative flow-rate dependence of the probability of traffic breakdown at a road bottleneck does not depend on the number of highway lanes (on features of lateral dynamics of vehicles), on the bottleneck type, and on real vehicle technology (during the last 30 years vehicle technology has changed considerably; however, qualitative empirical features of traffic breakdown did not change). In accordance with the three-phase theory that explains all known empirical features of traffic breakdown [33–35], the simple ACC model and TPACC model used in the paper reflect dynamic vehicle features that are responsible for traffic breakdown. For this reason, the result of the paper that at the same model parameters classic ACC vehicles (1) increase the breakdown probability whereas TPACC vehicles (4) decrease the breakdown probability proves that the use of indifference zones of the three-phase theory can have benefits for future automated driving. This is because contrarily with (1), human driving vehicles do not control time headway

within the time headway range (8) [33–35]. Thus, the TPACC vehicles, which can be considered automated driving "learning" from empirical human driving behavior, can decrease the breakdown probability.

Rather than an engineering work devoted to a development of the technology of self-driving vehicles, this work is a pure physical paper in which physical effects of the application of a simple TPACC model (4) have been presented. Results of this paper allow us to assume that future systems for automated driving should be developed whose rules are consistent with those of human driving vehicles. Otherwise, we could expect that automated driving vehicles can be considered as "obstacles" for drivers. The physics of automated driving in the framework of the three-phase theory studied in this paper emphasizes that future automated driving should be developed in which both the longitudinal dynamics (TPACC) and lateral dynamics should learn from driver behavior. In particular, the longitudinal and lateral dynamics of automated driving vehicles should be consistent with the existence of indifference zones of the three-phase theory [33–35,60].

### B. Conclusions

In the paper, based on numerical simulations of a simple model for automated driving in the framework of the three-phase theory (TPACC) introduced in the paper, we have found that applications of the TPACC strategy can lead to the following advantages in comparison with the classical approach to ACC:

(i) The absence of string instability.

(ii) Considerably smaller speed disturbances at road bottlenecks.

(iii) TPACC vehicles can decrease the probability of traffic breakdown at the bottleneck in mixed traffic flow; on the contrary, even a single automated driving vehicle based on the classical approach can provoke traffic breakdown at the bottleneck in mixed traffic flow.

These advantages of TPACC are associated with the absence of a fixed desired time headway to the preceding vehicle in the TPACC strategy: A TPACC vehicle exhibits a large indifference zone within the time headway range (8) within which the TPACC vehicle does not control time headway to the preceding vehicle. As we have found in this paper, due to the large indifference zone within the time headway range (8), the TPACC vehicle should not necessarily decelerate as strongly as the preceding vehicle when a local short-time speed disturbance appears at a road bottleneck. This dynamic behavior of TPACC vehicles decreases local speed disturbances in free flow at a road bottleneck. In its turn, the decrease in the amplitude of local speed disturbances at road bottlenecks results in a decrease in the probability of traffic breakdown in the traffic stream.

In this paper, we have made a comparison of the effect of classical ACC vehicles and TPACC vehicles on the probability of traffic breakdown at a road bottleneck in mixed traffic flow. In this scenario of the application of automated driving vehicles, we have considered only some specific values of TPACC and ACC parameters ($K_1$, $K_2$, and headway time) to demonstrate that the TPACC strategy can exhibit advantages in comparison with the classical ACC.

However, larger values of $K_1$ and $K_2$ and shorter headway time might give entirely different results. Moreover, the examples presented in the paper only involve situations where the total flow is near capacity. Thus, without exploring a wide range of scenarios we cannot make a general claim that the TPACC system is superior to ACC systems. Additionally, incorporating cooperative merging between ACC vehicles could reduce the tendency to initiate breakdown at highway bottlenecks. We believe that related detailed studies of the TPACC model introduced in the paper, which are out of the scope of this paper, will be a very interesting task of future investigations of the physics of automated driving.

## APPENDIX A: KERNER-KLENOV MICROSCOPIC STOCHASTIC TRAFFIC FLOW MODEL

In this appendix, we give explanations of the Kerner-Klenov stochastic microscopic three-phase model for human driving vehicles [66–68] and model parameters used for simulations of mixed traffic flow presented in the main text.

### 1. Complexity of real traffic observed in measured traffic data

The complexity of the Kerner-Klenov model [66–68] used for simulations of human driving vehicles is associated with the following complex spatiotemporal empirical features of real traffic flow observed in traffic data measured over many years in different countries [33]: Empirical spatiotemporal traffic data show that there are three phases in real traffic: free flow (F), synchronized flow (S), wide moving jam (J).

Between these traffic phases any combination of phase transitions is observed in real measured traffic data. In particular, an F $\rightarrow$ S transition determines traffic breakdown, whereas an S $\rightarrow$ J transition determines moving jam emergence. There can be spontaneous and induced phase transitions, i.e., the phase transitions occur in metastable states of associated traffic phases.

For a qualitative explanation of this empirical complexity of traffic, the author introduced a three-phase theory that is a qualitative traffic flow theory consisting of several hypotheses [33,60,62]. The Kerner-Klenov model [66–68] is a stochastic microscopic traffic flow model incorporating these hypotheses. The main objective of the model is to understand the physics of this empirical complexity of phase transitions and resulting spatiotemporal features of traffic patterns observed and measured in real traffic data.

### 2. Update rules of vehicle motion in road lane in model of identical drivers and vehicles

In a discrete model version of the Kerner-Klenov stochastic microscopic three-phase model used in all simulations presented in the main text, rather than the continuum space

coordinate [66], a discretized space coordinate with a small enough value of the discretization space interval $\delta x$ is used [68]. Consequently, the vehicle speed and acceleration (deceleration) discretization intervals are $\delta v = \delta x / \tau$ and $\delta a = \delta v / \tau$, respectively, where $\tau$ is the time step. Because in the discrete model version discrete (and dimensionless) values of the space coordinate, speed, and acceleration are used, which are measured respectively in values $\delta x$, $\delta v$, and $\delta a$, and time is measured in values of $\tau$, value $\tau$ in all formulas is assumed below to be the dimensionless value $\tau = 1$. In the discrete model version used for all simulations, the discretization cell $\delta x = 0.01$ m is used.

A choice of $\delta x = 0.01$ m made in the model determines the accuracy of vehicle speed calculations *in comparison* with the initial continuum in the space stochastic model of [66]. We have found that the discrete model exhibits similar characteristics of phase transitions and resulting congested patterns at highway bottlenecks as those in the continuum model at $\delta x$ that satisfies the conditions

$$\delta x / \tau^2 \ll b, a, a^{(a)}, a^{(b)}, a^{(0)}, \tag{A1}$$

where model parameters for driver deceleration and acceleration $b$, $a$, $a^{(a)}$, $a^{(b)}$, $a^{(0)}$ will be explained below.

Update rules of vehicle motion in the discrete model for identical drivers and identical vehicles moving in a road lane are as follows [68]:

$$v_{n+1} = \max(0, \min(v_{\text{free}}, \tilde{v}_{n+1} + \xi_n, v_n + a\tau, v_{\text{s},n})), \tag{A2}$$

$$x_{n+1} = x_n + v_{n+1}\tau, \tag{A3}$$

where the index $n$ corresponds to the discrete time $t_n = \tau n$, $n = 0, 1, \ldots$; $v_n$ is the vehicle speed at time step $n$, $a$ is the maximum acceleration, $\tilde{v}_n$ is the vehicle speed without speed fluctuations $\xi_n$:

$$\tilde{v}_{n+1} = \min(v_{\text{free}}, v_{\text{s},n}, v_{\text{c},n}), \tag{A4}$$

$$v_{\text{c},n} = \begin{cases} v_n + \Delta_n & \text{at} \quad g_n \leqslant G_n, \\ v_n + a_n\tau & \text{at} \quad g_n > G_n, \end{cases} \tag{A5}$$

$$\Delta_n = \max(-b_n\tau, \min(a_n\tau, v_{\ell,n} - v_n)), \tag{A6}$$

$$g_n = x_{\ell,n} - x_n - d, \tag{A7}$$

the subscript $\ell$ marks variables related to the preceding vehicle, $v_{\text{s},n}$ is a safe speed at time step $n$, $v_{\text{free}}$ is the free flow speed in free flow, $\xi_n$ describes speed fluctuations; $g_n$ is a space gap between two vehicles following each other; $G_n$ is the synchronization space gap; all vehicles have the same length $d$. The vehicle length $d$ includes the mean space gap between vehicles that are in a standstill within a wide moving jam. Values $a_n \geqslant 0$ and $b_n \geqslant 0$ in (A5), (A6) restrict changes in speed per time step when the vehicle accelerates or adjusts the speed to that of the preceding vehicle.

### 3. Synchronization space gap and hypothetical steady states of synchronized flow

Equations (A5), (A6) describe the adaptation of the vehicle speed to the speed of the preceding vehicle, i.e., the speed
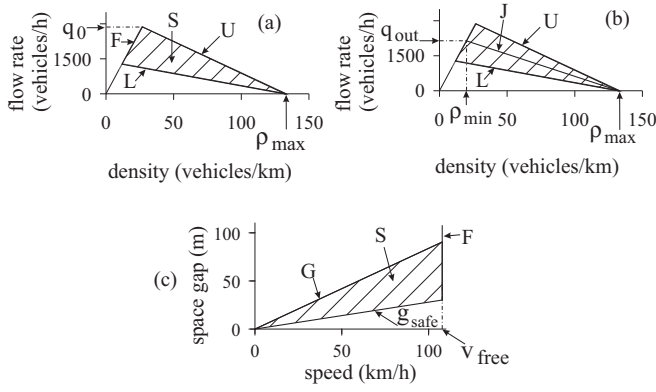
FIG. 11. Steady speed states for the Kerner-Klenov traffic flow model in the flow-density [(a), (b)] and in the space gap–speed planes (c). In (a), (b), $L$ and $U$ are, respectively, lower and upper boundaries of 2D regions of steady states of synchronized flow. In (b), J is the line $J$ whose slope is equal to the characteristic mean velocity $v_g$ of a wide moving jam; in the flow-density plane, the line $J$ represents the propagation of the downstream front of the wide moving jam with time-independent velocity $v_g$. F, free flow; S, synchronized flow.

adaptation effect in synchronized flow. This vehicle speed adaptation takes place within the synchronization gap $G_n$: At

$$g_n \leqslant G_n \tag{A8}$$

the vehicle tends to adjust its speed to the speed of the preceding vehicle. This means that the vehicle decelerates if $v_n > v_{\ell,n}$, and accelerates if $v_n < v_{\ell,n}$.

In (A5), the synchronization gap $G_n$ depends on the vehicle speed $v_n$ and on the speed of the preceding vehicle $v_{\ell,n}$:

$$G_n = G(v_n, v_{\ell,n}), \tag{A9}$$

$$G(u,w) = \max(0, \lfloor k\tau u + a^{-1}u(u-w)\rfloor), \tag{A10}$$

where $k > 1$ is constant; $\lfloor z \rfloor$ denotes the integer part of $z$.

The speed adaptation effect within the synchronization distance is related to the hypothesis of the three-phase theory: Hypothetical steady states of synchronized flow cover a 2D region in the flow-density plane [Fig. 11(a)]. Boundaries $F$, $L$, and $U$ of this 2D region shown in Fig. 11(a) are, respectively, associated with the free flow speed in free flow, a synchronization space gap $G$, and a safe space gap $g_{safe}$. A speed function of the safe space gap $g_{safe}(v)$ is found from the equation

$$v = v_s(g_{safe}, v). \tag{A11}$$

Respectively, as for the continuum model (see Sec. 16.3 of Ref. [33]), for the discrete model hypothetical steady states of synchronized flow cover a 2D region in the flow-density plane [Figs. 11(a), 11(b)]. However, because the speed $v$ and space gap $g$ are integer in the discrete model, the steady states do not form a continuum in the flow-density plane as they do in the continuum model. The inequalities

$$v \leqslant v_{free}, \quad g \leqslant G(v,v), \quad g \geqslant g_{safe}(v) \tag{A12}$$

define a 2D region in the space gap–speed plane [Fig. 11(c)] in which the hypothetical steady states exist for the discrete model, when all model fluctuations are neglected.

In (A12), we have taken into account that in the hypothetical steady states of synchronized flow vehicle speeds and space gaps are assumed to be time-independent and the speed of each of the vehicles is equal to the speed of the associated preceding vehicle: $v = v_\ell$. However, due to model fluctuations, steady states of synchronized flow are destroyed; i.e., they do not exist in simulations. This explains the term "hypothetical" steady states of synchronized flow. Therefore, rather than steady states, some nonhomogeneous in space and time traffic states occur. In other words, steady states are related to a hypothetical model-fluctuation-less limit of homogeneous in space and time vehicle motion that is not realized in real simulations. Driver time delays are described through model fluctuations. Therefore, any application of the Kerner-Klenov stochastic microscopic three-phase traffic flow model without model fluctuations has *no sense*. In other words, for the description of real spatiotemporal traffic flow phenomena, model speed fluctuations incorporated in this model are needed.

### 4. Model speed fluctuations

In the model, random vehicle deceleration and acceleration are applied depending on whether the vehicle decelerates or accelerates, or else maintains its speed:

$$\xi_n = \begin{cases} \xi_a, & \text{if } S_{n+1} = 1, \\ -\xi_b, & \text{if } S_{n+1} = -1, \\ \xi^{(0)}, & \text{if } S_{n+1} = 0. \end{cases} \tag{A13}$$

State of vehicle motion $S_{n+1}$ in (A13) is determined by formula

$$S_{n+1} = \begin{cases} -1, & \text{if } \tilde{v}_{n+1} < v_n, \\ 1, & \text{if } \tilde{v}_{n+1} > v_n, \\ 0, & \text{if } \tilde{v}_{n+1} = v_n. \end{cases} \tag{A14}$$

In (A13), $\xi_b$, $\xi^{(0)}$, and $\xi_a$ are random sources for deceleration and acceleration that are as follows:

$$\xi_b = a^{(b)}\tau\Theta(p_b - r), \tag{A15}$$

$$\xi^{(0)} = a^{(0)}\tau \begin{cases} -1, & \text{if } r < p^{(0)}, \\ 1, & \text{if } p^{(0)} \leqslant r < 2p^{(0)} \text{ and } v_n > 0, \\ 0, & \text{otherwise}, \end{cases} \tag{A16}$$

$$\xi_a = a^{(a)}\tau\Theta(p_a - r); \tag{A17}$$

$p_b$ is the probability of random vehicle deceleration, $p_a$ is the probability of random vehicle acceleration, $p^{(0)}$ and $a^{(0)} \leqslant a$ are constants, $r = \mathrm{rand}(0,1)$, $\Theta(z) = 0$ at $z < 0$ and $\Theta(z) = 1$ at $z \geqslant 0$, $a^{(a)}$ and $a^{(b)}$ are model parameters (see Table I), which in some applications can be chosen as speed functions $a^{(a)} = a^{(a)}(v_n)$ and $a^{(b)} = a^{(b)}(v_n)$.

TABLE I. Model parameters of vehicle motion in road lane used in simulations of the main text.

$\tau_{\text{safe}} = \tau = 1$ s, $d = 7.5$ m$/\delta x$,
$\delta x = 0.01$ m, $\delta v = 0.01$ m s$^{-1}$, $\delta a = 0.01$ m s$^{-2}$,
$v_{\text{free}} = 30$ m s$^{-1}/\delta v$, $b = 1$ m s$^{-2}/\delta a$, $a = 0.5$ m s$^{-2}/\delta a$,
$k = 3$, $p_1 = 0.3$, $p_b = 0.1$, $p_a = 0.17$, $p^{(0)} = 0.005$,
$p_0(v_n) = 0.575 + 0.125 \min(1, v_n/v_{01})$,
$p_2(v_n) = 0.48 + 0.32\Theta(v_n - v_{21})$,
$v_{01} = 10$ m s$^{-1}/\delta v$, $v_{21} = 15$ m s$^{-1}/\delta v$,
$a^{(0)} = 0.2a$, $a^{(a)} = a^{(b)} = a$

### 5. Stochastic time delays of acceleration and deceleration

To simulate time delays either in vehicle acceleration or in vehicle deceleration, $a_n$ and $b_n$ in (A6) are taken as the following stochastic functions:

$$a_n = a\Theta(P_0 - r_1), \tag{A18}$$

$$b_n = a\Theta(P_1 - r_1), \tag{A19}$$

$$P_0 = \begin{cases} p_0, & \text{if } S_n \neq 1, \\ 1, & \text{if } S_n = 1, \end{cases} \tag{A20}$$

$$P_1 = \begin{cases} p_1, & \text{if } S_n \neq -1, \\ p_2, & \text{if } S_n = -1; \end{cases} \tag{A21}$$

$r_1 = \text{rand}(0,1)$, $p_1$ is constant, $p_0 = p_0(v_n)$ and $p_2 = p_2(v_n)$ are speed functions (see Table I).

### 6. Simulations of slow-to-start rule

In the model, simulations of the well-known effect of the driver time delay in acceleration at the downstream front of synchronized flow or a wide moving jam known as a slow-to-start rule [131,132] are made as a collective effect through the use of Eqs. (A5), (A6), and a random value of vehicle acceleration (A18). Equation (A18) with $P_0 = p_0 < 1$ is applied only if the vehicle did not accelerate at the former time step ($S_n \neq 1$); in the latter case, a vehicle accelerates with some probability $p_0$ that depends on the speed $v_n$; otherwise $P_0 = 1$ [see formula (A20)].

The mean time delay in vehicle acceleration is equal to

$$\tau_{\text{del}}^{(\text{acc})}(v_n) = \frac{\tau}{p_0(v_n)}. \tag{A22}$$

From formula (A22), it follows that the mean time delay in vehicle acceleration from a standstill within a wide moving jam [i.e., when in formula (A22) the speed $v_n = 0$] is equal to

$$\tau_{\text{del}}^{(\text{acc})}(0) = \frac{\tau}{p_0(0)}. \tag{A23}$$

The mean time delay in vehicle acceleration from a standstill within a wide moving jam determines the parameters of the line $J$ in the flow-density plane [Fig. 11(b)].

Probability $p_0(v_n)$ in (A20) is chosen to be an increasing speed function (see Table I). Because the speed within synchronized flow is larger than zero, the mean time delay in vehicle acceleration at the downstream front of synchronized flow that

we denote by

$$\tau_{\text{del, syn}}^{(\text{acc})} = \tau_{\text{del}}^{(\text{acc})}(v_n), \quad v_n > 0, \tag{A24}$$

is shorter than the mean time delay in vehicle acceleration at the downstream front of the wide moving jam $\tau_{\text{del}}^{(\text{acc})}(0)$:

$$\tau_{\text{del, syn}}^{(\text{acc})} < \tau_{\text{del}}^{(\text{acc})}(0). \tag{A25}$$

### 7. Safe speed

In the model, the safe speed $v_{s,n}$ in (A2) is chosen in the form

$$v_{s,n} = \min\left(v_n^{(\text{safe})}, g_n/\tau + v_\ell^{(a)}\right), \tag{A26}$$

$v_\ell^{(a)}$ is an "anticipation" speed of the preceding vehicle that will be considered below, the function

$$v_n^{(\text{safe})} = \lfloor v^{(\text{safe})}(g_n, v_{\ell,n}) \rfloor \tag{A27}$$

in (A26) is related to the safe speed $v^{(\text{safe})}(g_n, v_{\ell,n})$ in the model by Krauß *et al.* [133], which is a solution of the Gipps's equation [134]

$$v^{(\text{safe})}\tau + X_{\text{d}}(v^{(\text{safe})}) = g_n + X_{\text{d}}(v_{\ell,n}), \tag{A28}$$

where $X_{\text{d}}(u)$ is the braking distance that should be passed by the vehicle moving first with the speed $u$ before the vehicle can come to a stop.

The condition (A28) enables us to find the safe speed $v^{(\text{safe})}$ as a function of the space gap $g_n$ and speed $v_{\ell,n}$ provided $X_{\text{d}}(u)$ is a known function. In the case when the vehicle brakes with a constant deceleration $b$, the change in the vehicle speed for each time step is $-b\tau$ except the last time step before the vehicle comes to a stop. At the last time step, the vehicle decreases its speed at the value $b\tau\beta$, where $\beta$ is a fractional part of $u/b\tau$. According to formula (A3) for the displacement of the vehicle for one time step, the braking distance $X_{\text{d}}(u)$ is [133]

$$X_{\text{d}}(u) = \tau(u - b\tau + u - 2b\tau + \cdots + \beta b\tau). \tag{A29}$$

From (A29), it follows [133]

$$X_{\text{d}}(u) = b\tau^2\left[\alpha\beta + \frac{\alpha(\alpha - 1)}{2}\right]; \tag{A30}$$

$\alpha = \lfloor u/b\tau \rfloor$ is an integer part of $u/b\tau$.

The safe speed $v^{(\text{safe})}$ as a solution of Eq. (A28) at the distance $X_{\text{d}}(u)$ given by (A30) has been found by Krauß *et al.* [133]:

$$v^{(\text{safe})}(g_n, v_{\ell,n}) = b\tau(\alpha_{\text{safe}} + \beta_{\text{safe}}), \tag{A31}$$

where

$$\alpha_{\text{safe}} = \left\lfloor \sqrt{2\frac{X_{\text{d}}(v_{\ell,n}) + g_n}{b\tau^2} + \frac{1}{4}} - \frac{1}{2} \right\rfloor, \tag{A32}$$

$$\beta_{\text{safe}} = \frac{X_{\text{d}}(v_{\ell,n}) + g_n}{(\alpha_{\text{safe}} + 1)b\tau^2} - \frac{\alpha_{\text{safe}}}{2}. \tag{A33}$$

The safe speed in the model by Krauß *et al.* [133] provides collisionless motion of vehicles if the time gap $g_n/v_n$ between two vehicles is greater than or equal to the time step $\tau$, i.e., if $g_n \geqslant v_n\tau$ [135]. In the model, it is assumed that in some cases, mainly due to lane changing or merging of vehicles onto the main road within the merging region of bottlenecks, the space

gap $g_n$ can become less than $v_n \tau$. In these critical situations, the collisionless motion of vehicles in the model is a result of the second term in (A26) in which some prediction $(v_\ell^{(a)})$ of the speed of the preceding vehicle at the next time step is used. The related "anticipation" speed $v_\ell^{(a)}$ at the next time step is given by formula

$$v_\ell^{(a)} = \max\left(0, \min\left(v_{\ell,n}^{(safe)}, v_{\ell,n}, g_{\ell,n}/\tau\right) - a\tau\right), \quad \text{(A34)}$$

where $v_{\ell,n}^{(safe)}$ is the safe speed (A27), (A31)–(A33) for the preceding vehicle, $g_{\ell,n}$ is the space gap in front of the preceding vehicle. Simulations have shown that formulas (A26), (A27), (A31)–(A34) lead to collisionless vehicle motion over a wide range of parameters of the merging region of on-ramp bottlenecks (Appendix C).

In hypothetical steady states of traffic flow [Fig. 11(a)], the safe space gap $g_{safe}$ is determined from equation $v = v_s$; in accordance with Eqs. (A26)–(A28), at a given $v$ in steady traffic states $v = v_\ell$ the safe speed

$$v_s = g_{safe}/\tau_{safe}, \quad \text{(A35)}$$

and, therefore,

$$g_{safe} = v\tau_{safe}. \quad \text{(A36)}$$

### 8. Boundary and initial conditions

Open boundary conditions are applied. At the beginning of the road new vehicles are generated one after another in each of the lanes of the road at time moments

$$t^{(m)} = \tau\lceil m\tau_{in}/\tau\rceil, \quad m = 1, 2, \ldots. \quad \text{(A37)}$$

In (A37), $\tau_{in} = 1/q_{in}$, $q_{in}$ is the flow rate in the incoming boundary flow per lane, $\lceil z \rceil$ denotes the nearest integer greater than or equal to $z$. A new vehicle appears on the road only if the distance from the beginning of the road ($x = x_b$) to the position $x = x_{\ell,n}$ of the farthest upstream vehicle on the road is not smaller than the safe distance $v_{\ell,n}\tau + d$:

$$x_{\ell,n} - x_b \geqslant v_{\ell,n}\tau + d, \quad \text{(A38)}$$

where $n = t^{(m)}/\tau$. Otherwise, condition (A38) is checked at time $(n + 1)\tau$ that is the next one to time $t^{(m)}$ (A37), and so on, until the condition (A38) is satisfied. Then the next vehicle appears on the road. After this occurs, the number $m$ in (A37) is increased by 1.

The speed $v_n$ and coordinate $x_n$ of the new vehicle are

$$v_n = v_{\ell,n},$$
$$x_n = \max(x_b, x_{\ell,n} - \lfloor v_n\tau_{in}\rfloor). \quad \text{(A39)}$$

The flow rate $q_{in}$ is chosen to have the value $v_{free}\tau_{in}$ integer. In the initial state ($n = 0$), all vehicles have the free flow speed $v_n = v_{free}$ and they are positioned at space intervals $x_{\ell,n} - x_n = v_{free}\tau_{in}$.

After a vehicle has reached the end of the road it is removed. Before this occurs, the farthest downstream vehicle maintains its speed and lane. For the vehicle following the farthest downstream one, the "anticipation" speed $v_\ell^{(a)}$ in (A26) is equal to the speed of the farthest downstream vehicle.

In [35] it has been shown that the Kerner-Klenov model (A2)–(A7), (A9), (A10), (A13)–(A21), (A26), (A27), (A31)–(A34) is a Markov chain: At time step $n + 1$, values of model

variables $v_{n+1}$, $x_{n+1}$, and $S_{n+1}$ are calculated based only on their values $v_n$, $x_n$, and $S_n$ at step $n$.

## APPENDIX B: MODEL OF CLASSICAL ACC

In simulations of the classical ACC model (1), as in the model of human driving vehicles (Appendix A 2) we use the discrete time $t = n\tau$, where $n = 0, 1, 2, \ldots$; $\tau = 1$ s is time step. Therefore, the space gap to the preceding vehicle is equal to $g_n = x_{\ell,n} - x_n - d$ and the relative speed is given by $\Delta v_n = v_{\ell,n} - v_n$, where $x_n$ and $v_n$ are coordinate and speed of the ACC vehicle, $x_{\ell,n}$ and $v_{\ell,n}$ are coordinate and speed of the preceding vehicle, $d$ is the vehicle length that is assumed the same one for automated driving and human driving vehicles. Correspondingly, the classical model of the dynamics of ACC vehicle (1) can be rewritten as follows [35]:

$$a_n^{(ACC)} = K_1\left(g_n - v_n\tau_d^{(ACC)}\right) + K_2(v_{\ell,n} - v_n). \quad \text{(B1)}$$

The ACC vehicles move in accordance with Eq. (B1) where, in addition, the following formulas are used:

$$v_{c,n}^{(ACC)} = v_n + \tau\max\left(-b_{max}, \min\left(\lfloor a_n^{(ACC)}\rfloor, a_{max}\right)\right), \quad \text{(B2)}$$

$$v_{n+1} = \max\left(0, \min\left(v_{free}, v_{c,n}^{(ACC)}, v_{s,n}\right)\right); \quad \text{(B3)}$$

$\lfloor z \rfloor$ denotes the integer part of $z$ [128]. Through the use of formula (B2), acceleration and deceleration of the ACC vehicles are limited by some maximum acceleration $a_{max}$ and maximum deceleration $b_{max}$, respectively. Owing to the formula (B3), the speed of the ACC vehicle $v_{n+1}$ at time step $n + 1$ is limited by the maximum speed in free flow $v_{free}$ and by the safe speed $v_{s,n}$ to avoid collisions between vehicles [136]. The maximum speed in free flow $v_{free}$ and the safe speed $v_{s,n}$ are chosen, respectively, the same as those in the microscopic model of human driving vehicles (Appendix A 2). It should be noted that the model of the ACC vehicle merging from the on-ramp onto the main road is similar to that for human driving vehicles (see Appendix C 2).

## APPENDIX C: MODEL OF ON-RAMP BOTTLENECK

An on-ramp bottleneck consists of two parts (Fig. 12):

(i) The merging region of length $L_m$ where vehicles can merge onto the main road from the on-ramp lane.

(ii) A part of the on-ramp lane of length $L_r$ upstream of the merging region where vehicles move in accordance with the model of Appendix A 2. The maximal speed of vehicles is $v_{free} = v_{free\,on}$.

At the beginning of the on-ramp lane ($x = x_{on}^{(b)}$) the flow rate to the on-ramp $q_{on}$ is given through boundary conditions
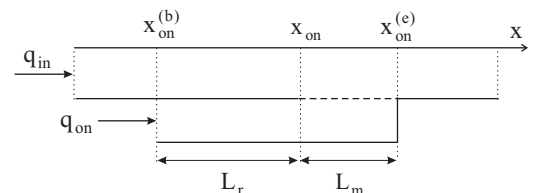


FIG. 12. Model of on-ramp bottleneck on single-lane road.

TABLE II. Parameters of model of on-ramp bottleneck used in simulations of the main text.

| |
| --- |
| $\lambda_{\rm b} = 0.75$, |
| $v_{\rm free\ on} = 22.2$ m s$^{-1}/\delta v$, |
| $\Delta v_r^{(2)} = 5$ m s$^{-1}/\delta v$, |
| $L_{\rm r} = 1$ km$/\delta x$, $\Delta v_{\rm r}^{(1)} = 10$ m s$^{-1}/\delta v$, |
| $L_{\rm m} = 0.3$ km$/\delta x$ |

that are the same as those that determine the flow rate $q_{\rm in}$ at the beginning of the main road (Appendix A 8).

### 1. Model of vehicle merging at bottleneck

#### a. Vehicle speed adaptation within merging region of bottleneck

For the on-ramp bottleneck, when a vehicle is within the merging region of the bottleneck, the vehicle takes into account the space gaps to the preceding vehicles and their speeds both in the current and target lanes. Respectively, instead of formula (A5), in (A4) for the speed $v_{{\rm c},n}$ the following formula is used:

$$v_{{\rm c},n} = \begin{cases} v_n + \Delta_n^+ & \text{at } g_n^+ \leqslant G(v_n, \hat{v}_n^+), \\ v_n + a_n\tau & \text{at } g_n^+ > G(v_n, \hat{v}_n^+), \end{cases} \tag{C1}$$

$$\Delta_n^+ = \max(-b_n\tau, \min(a_n\tau, \hat{v}_n^+ - v_n)), \tag{C2}$$

$$\hat{v}_n^+ = \max\left(0, \min\left(v_{\rm free}, v_n^+ + \Delta v_r^{(2)}\right)\right); \tag{C3}$$

$\Delta v_r^{(2)}$ is constant (see Table II).

Superscripts $+$ and $-$ in variables, parameters, and functions denote the preceding vehicle and the trailing vehicle in the "target" (neighboring) lane, respectively. The target lane is the lane into which the vehicle wants to change.

The safe speed $v_{{\rm s},n}$ in (A2), (A4) for the vehicle that is the closest one to the end of the merging region is chosen in the form

$$v_{{\rm s},n} = \left\lfloor v^{({\rm safe})}\left(x_{\rm on}^{({\rm e})} - x_n, 0\right) \right\rfloor \tag{C4}$$

(see Fig. 12 and Table II).

#### b. Safety conditions for vehicle merging

Vehicle merging at the bottleneck occurs when safety conditions ($*$) *or* safety conditions ($**$) are satisfied.

Safety conditions ($*$) are as follows:

$$g_n^+ > \min(\hat{v}_n\tau, G(\hat{v}_n, v_n^+)),$$
$$g_n^- > \min(v_n^-\tau, G(v_n^-, \hat{v}_n)), \tag{C5}$$

$$\hat{v}_n = \min\left(v_n^+, v_n + \Delta v_r^{(1)}\right); \tag{C6}$$

$\Delta v_r^{(1)} > 0$ is constant (see Table II).

Safety conditions ($**$) are as follows:

$$x_n^+ - x_n^- - d > g_{\rm target}^{(\min)}, \tag{C7}$$

where

$$g_{\rm target}^{(\min)} = \lfloor \lambda_{\rm b} v_n^+ + d \rfloor; \tag{C8}$$

$\lambda_{\rm b}$ is constant. In addition to conditions (C7), the safety condition ($**$) includes the condition that the vehicle should

pass the midpoint

$$x_n^{({\rm m})} = \lfloor (x_n^+ + x_n^-)/2 \rfloor \tag{C9}$$

between two neighboring vehicles in the target lane; i.e., conditions

$$x_{n-1} < x_{n-1}^{({\rm m})} \text{ and } x_n \geqslant x_n^{({\rm m})}$$
$$\text{or}$$
$$x_{n-1} \geqslant x_{n-1}^{({\rm m})} \text{ and } x_n < x_n^{({\rm m})} \tag{C10}$$

should also be satisfied.

#### c. Speed and coordinate of vehicle after vehicle merging

The vehicle speed after vehicle merging is equal to

$$v_n = \hat{v}_n. \tag{C11}$$

Under conditions ($*$), the vehicle coordinate $x_n$ remains the same. Under conditions ($**$), the vehicle coordinate $x_n$ is equal to

$$x_n = x_n^{({\rm m})}. \tag{C12}$$

### 2. Merging of ACC vehicle or TPACC vehicle at on-ramp bottleneck

Here we consider rules of the merging of an ACC vehicle at the on-ramp bottleneck presented in [35] and used in simulations. The same rules have also been used in simulations of the merging of an TPACC vehicle from the on-ramp lane onto the main road at the bottleneck.

In the on-ramp lane, an ACC vehicle or a TPACC vehicle moves in accordance with the ACC model (B1)–(B3) or in accordance with the TPACC model (5)–(7) of the main text, respectively. The maximal speed of the ACC vehicle or the TPACC vehicle in the on-ramp lane is $v_{\rm free} = v_{\rm free\ on}$. The safe speed $v_{{\rm s},n}$ in (B3) for the ACC vehicle and in (7) for the TPACC vehicle that is the closest one to the end of the merging region is the same as that for human driving vehicles that is given by formula (C4).

An ACC vehicle or a TPACC vehicle merges from the on-ramp lane onto the main road, when some safety conditions ($*$) *or* safety conditions ($**$) are satisfied for the ACC vehicle or the TPACC vehicle. Safety conditions ($*$) for ACC vehicles and TPACC vehicles are as follows:

$$g_n^+ > \hat{v}_n\tau, \quad g_n^- > v_n^-\tau, \tag{C13}$$

where $\hat{v}_n$ is given by formula (C6). Safety conditions ($**$) are given by formulas (C7)–(C10); i.e., they are the same as those for human driving vehicles. Respectively, as for human driving vehicles, the ACC vehicle speed and its coordinate or the TPACC vehicle speed and its coordinate after the ACC vehicle or the TPACC vehicle has merged from the on-ramp onto the main road are determined by formulas (C11) and (C12).

[1] *Automated Highway Systems*, edited by P. A. Ioannou (Plenum Press, New York, 1997).

[2] P. A. Ioannou and J. Sun, *Robust Adaptive Control* (Prentice Hall, Inc., Upper Saddle River, New Jersey, 1996).

[3] P. A. Ioannou and E. B. Kosmatopoulos, in *Wiley Encyclopedia of Electrical and Electronics Engineering*, edited by J. G. Webster (John Wiley & Sons, Inc., New York, 2000).

[4] W. Levine and M. Athans, IEEE Trans. Automat. Contr. **11**, 355 (1966).

[5] C.-Y. Liang and H. Peng, Veh. Syst. Dyn. **32**, 313 (1999).

[6] C.-Y. Liang and H. Peng, JSME Intl. J., Ser. C: Mech. Syst., Mach. Elem. Manuf. **43**, 671 (2000).

[7] R. Rajamani, *Vehicle Dynamics and Control*, Mechanical Engineering Series (Springer US, Boston, MA, 2012).

[8] G. Meyer and S. Beiker, *Road Vehicle Automation* (Springer, Berlin, 2014).

[9] K. Bengler, K. Dietmayer, B. Farber, M. Maurer, Ch. Stiller, and H. Winner, IEEE Intelligent Transp. Sys. Magazine **6**, 6 (2014).

[10] *Autonomes Fahren*, edited by M. Maurer, J. Ch. Gerdes, B. Lenz, and H. Winner (Springer-Verlag, Berlin, 2015).

[11] D. Swaroop and J. K. Hedrick, IEEE Trans. Automat. Contr. **41**, 349 (1996).

[12] D. Swaroop, J. K. Hedrick, and S. B. Choi, IEEE Trans. Veh. Technol. **50**, 150 (2001).

[13] P. Ioannou and C. C. Chien, IEEE Trans. Veh. Technol. **42**, 657 (1993).

[14] P. Varaiya, IEEE Trans. Autom. Control **38**, 195 (1993).

[15] L. C. Davis, Phys. Rev. E **69**, 066110 (2004).

[16] L. C. Davis, Physica A **405**, 128 (2014).

[17] Automated Highway Systems, http://www.seminarsonly.com/Civil_Engineering/automated-highway-systems.php.

[18] Automated Highway Systems, https://seminarprojects.blogspot.de/2012/01/detailed-report-on-automated-highway.html.

[19] European Roadmap Smart Systems for Automated Driving, https://www.smart-systems-integration.org/public/documents.

[20] Automatisches Fahren, http://www.tuvpt.de/index.php?id=foerderung000.

[21] S. E. Shladover, Veh. Syst. Dyn. **24**, 551 (1995).

[22] A. D. May, *Traffic Flow Fundamentals* (Prentice-Hall, Inc., Englewood Cliffs, New Jersey, 1990).

[23] *Highway Capacity Manual 2000* (National Research Council, Transportation Research Board, Washington, DC, 2000).

[24] *Highway Capacity Manual 2010* (National Research Council, Transportation Research Board, Washington, DC, 2010).

[25] L. Elefteriadou, *An Introduction to Traffic Flow Theory*, Springer Optimization and Its Applications (Springer, Berlin, 2014), Vol. 84.

[26] M. Brackstone and M. McDonald, Transp. Res. F **2**, 181 (1998).

[27] D. C. Gazis, *Traffic Theory* (Springer, Berlin, 2002).

[28] A. Schadschneider, D. Chowdhury, and K. Nishinari, *Stochastic Transport in Complex Systems* (Elsevier Science, Inc., New York, 2011).

[29] D. Helbing, Rev. Mod. Phys. **73**, 1067 (2001).

[30] T. Nagatani, Rep. Prog. Phys. **65**, 1331 (2002).

[31] K. Nagel, P. Wagner, and R. Woesler, Oper. Res. **51**, 681 (2003).

[32] M. Treiber and A. Kesting, *Traffic Flow Dynamics* (Springer, Heidelberg, 2013).

[33] B. S. Kerner, *The Physics of Traffic* (Springer, Berlin, 2004).

[34] B. S. Kerner, *Introduction to Modern Traffic Flow Theory and Control* (Springer, Berlin, 2009).

[35] B. S. Kerner, *Breakdown in Traffic Networks* (Springer, Berlin, 2017).

[36] L. Elefteriadou, R. P. Roess, and W. R. McShane, Transp. Res. Rec. **1484**, 80 (1995).

[37] B. N. Persaud, S. Yagar, and R. Brownlee, Trans. Res. Rec. **1634**, 64 (1998).

[38] S. Dharba and K. R. Rajagopal, Transp. Res. C **7**, 329 (1999).

[39] G. Marsden, M. McDonald, and M. Brackstone, Transp. Res. C **9**, 33 (2001).

[40] J. VanderWerf, S. E. Shladover, N. Kourjanskaia, M. Miller, and H. Krishnan, Transp. Res. Rec. **1748**, 167 (2001).

[41] J. VanderWerf, S. E. Shladover, M. A. Miller, and N. Kourjanskaia, Transp. Res. Rec. **1800**, 78 (2002).

[42] M. Treiber and D. Helbing, Automatisierungstechnik **49**, 478 (2001).

[43] P. Y. Li and A. Shrivastava, Transp. Res. C **10**, 275 (2002).

[44] S. Kukuchi, N. Uno, and M. Tanaka, J. Transp. Eng. **129**, 146 (2003).

[45] A. Bose and P. Ioannou, Transp. Res. C **11**, 439 (2003).

[46] H. Suzuki, JSAE Rev. **24**, 403 (2003).

[47] J. Zhou and H. Peng, IEEE Trans. Intell. Transp. Syst. **6**, 229 (2005).

[48] B. van Arem, C. J. G. van Driel, and R. Visser, IEEE Trans. Intell. Transp. Syst. **7**, 429 (2006).

[49] J.-J. Martinez and C. Canudas-do-Wit, IEEE Trans. Control Syst. Technol. **15**, 246 (2007).

[50] A. Kesting, M. Treiber, M. Schönhof, and D. Helbing, Transp. Res. Rec. **2000**, 16 (2007).

[51] A. Kesting, M. Treiber, M. Schönhof, and D. Helbing, Transp. Res. C **16**, 668 (2008).

[52] T.-W. Lin, S.-L. Hwang, and P. Green, Safety Sci. **47**, 620 (2009).

[53] S. E. Shladover, D. Su, and X.-T. Lu, Transp. Res. Rec. **2324**, 63 (2012).

[54] D. Ngoduy, Transpormetrica **8**, 43 (2012).

[55] D. Ngoduy, Commun. Nonlinear Sci. Numer. Simulat. **18**, 2838 (2013).

[56] A. I. Delis, I. K. Nikolos, and M. Papageorgiou, Comput. Math. Appl. **70**, 1921 (2015).

[57] I. A. Ktousakis, I. K. Nokolos, and M. Papageorgiou, Transp. Res. Procedia **6**, 111 (2015).

[58] A. Talebpour and H. S. Mahmassani, Transp. Res. C **71**, 143 (2016).

[59] R. Wang, Y. Li, and D. B. Work, Transp. Res. C **78**, 95 (2017).

[60] B. S. Kerner, Phys. Rev. Lett. **81**, 3797 (1998); Trans. Res. Rec. **1678**, 160 (1999); in *Transportation and Traffic Theory*, edited by A. Ceder (Elsevier Science, Amsterdam, 1999), pp. 147–171; B. S. Kerner, Phys. World **12**, 25 (1999).

[61] B. S. Kerner, M. Koller, S. L. Klenov, H. Rehborn, and M. Leibel, Physica A **438**, 365 (2015).

[62] The main prediction of the three-phase theory is the nucleation nature of the S → F instability that governs the metastability of free flow with respect to the F → S transition at the bottleneck [33,60,63]. The S → F instability and the associated metastability of free flow with respect to the F → S transition at the bottleneck have no sense for the classical traffic and transportation theories. Therefore, the three-phase theory is

incommensurable with all earlier traffic flow theories and models (for a review, see [35]).

[63] B. S. Kerner, Phys. Rev. E **92**, 062827 (2015).

[64] B. S. Kerner, Physica A **392**, 5261 (2013); Elektrot. Informat. **132**, 417 (2015).

[65] B. S. Kerner, Physica A **450**, 700 (2016).

[66] B. S. Kerner and S. L. Klenov, J. Phys. A: Math. Gen. **35**, L31 (2002).

[67] B. S. Kerner and S. L. Klenov, Phys. Rev. E **68**, 036130 (2003).

[68] B. S. Kerner and S. L. Klenov, Phys. Rev. E **80**, 056101 (2009).

[69] B. S. Kerner, German patent publication DE 10308256A1 (2004); Patent WO 2004076223A1 (2004); EU Patent EP 1597106B1 (2006); German patent DE 502004001669D1 (2006); USA patent US 20070150167A1 (2007); USA patent US 7451039B2 (2008); German patent publication DE 102007008253A1 (2007); German patent publication DE 102007008257A1 (2007); German patent publication DE 102007008254A1 (2008).

[70] The main reason for the use of the word "three phase" in the ACC strategy is as follows. A 2D region of operating points of TPACC (Figs. 1 and 2) follows from the driver behavior first incorporated in the three-phase theory in which a 2D region of steady states of synchronized flow is assumed [60]. The word "three phase" for TPACC should emphasize both a qualitative difference between the two types of ACCs and the fact that the idea of TPACC with no fixed time headway to the preceding vehicle has been taken from the three-phase theory.

[71] Since the Kerner-Klenov car-following model with indifference zones in car following based on the three-phase theory (dashed region in Fig. 1) was introduced [66] (in this paper, a discrete version of this model [68] has been used), a number of different traffic flow models incorporating some of the hypotheses of the three-phase theory have been developed and many results with the use of these models have been found (e.g., [15,16,67,72–124]).

[72] B. S. Kerner, S. L. Klenov, and D. E. Wolf, J. Phys. A: Math. Gen. **35**, 9971 (2002).

[73] L. C. Davis, Phys. Rev. E **69**, 016108 (2004).

[74] L. C. Davis, Physica A **368**, 541 (2006).

[75] L. C. Davis, Physica A **379**, 274 (2007).

[76] H. K. Lee, R. Barlović, M. Schreckenberg, and D. Kim, Phys. Rev. Lett. **92**, 238702 (2004).

[77] R. Jiang and Q.-S. Wu, J. Phys. A: Math. Gen. **37**, 8197 (2004).

[78] K. Gao, R. Jiang, S.-X. Hu, B.-H. Wang, and Q.-S. Wu, Phys. Rev. E **76**, 026105 (2007).

[79] L. C. Davis, Physica A **361**, 606 (2006).

[80] L. C. Davis, Physica A **387**, 6395 (2008).

[81] L. C. Davis, Physica A **388**, 4459 (2009).

[82] L. C. Davis, Physica A **389**, 3588 (2010).

[83] L. C. Davis, Physica A **391**, 1679 (2012).

[84] R. Jiang, M.-B. Hua, R. Wang, and Q.-S. Wu, Phys. Lett. A **365**, 6 (2007).

[85] R. Jiang and Q.-S. Wu, Phys. Rev. E **72**, 067103 (2005).

[86] R. Jiang and Q.-S. Wu, Physica A **377**, 633 (2007).

[87] R. Wang, R. Jiang, Q.-S. Wu, and M. Liu, Physica A **378**, 475 (2007).

[88] A. Pottmeier, C. Thiemann, A. Schadschneider, and M. Schreckenberg, in *Traffic and Granular Flow '05*, edited by A. Schadschneider, T. Pöschel, R. Kühne, M. Schreckenberg, and D. E. Wolf (Springer, Berlin, 2007), pp. 503–508.

[89] X. G. Li, Z. Y. Gao, K. P. Li, and X. M. Zhao, Phys. Rev. E **76**, 016110 (2007).

[90] J. J. Wu, H. J. Sun, and Z. Y. Gao, Phys. Rev. E **78**, 036103 (2008).

[91] J. A. Laval, in *Traffic and Granular Flow '05*, edited by A. Schadschneider, T. Pöschel, R. Kühne, M. Schreckenberg, and D. E. Wolf (Springer, Berlin, 2007), pp. 521–526.

[92] S. Hoogendoorn, H. van Lint, and V. L. Knoop, Trans. Res. Rec. **2088**, 102 (2008).

[93] K. Gao, R. Jiang, B.-H. Wang, and Q.-S. Wu, Physica A **388**, 3233 (2009).

[94] B. Jia, X.-G. Li, T. Chen, R. Jiang, and Z.-Y. Gao, Transportmetrica **7**, 127 (2011).

[95] J.-F. Tian, B. Jia, X.-G. Li, R. Jiang, X.-M. Zhao, and Z.-Y. Gao, Physica A **388**, 4827 (2009).

[96] S. He, W. Guan, and L. Song, Physica A **389**, 825 (2009).

[97] C.-J. Jin, W. Wang, R. Jiang, and K. Gao, J. Stat. Mech. (2010) P03018.

[98] S. L. Klenov, in Proc. of Moscow Inst. of Phys. and Technology (State University), edited by V. V. Kozlov, Vol. 2, 2010, pp. 75–90 (in Russian).

[99] A. V. Gasnikov, S. L. Klenov, E. A. Nurminski, Y. A. Kholodov, and N. B. Shamray, Introduction to mathematical simulations of traffic flow, Moscow, MCNMO, 2013 (in Russian).

[100] S. Kokubo, J. Tanimoto, and A. Hagishima, Physica A **390**, 561 (2011).

[101] H.-K. Lee and B.-J. Kim, Physica A **390**, 4555 (2011).

[102] C.-J. Jin and W. Wang, Physica A **390**, 4184 (2011).

[103] J. P. L. Neto, M. L. Lyra, and C. R. da Silva, Physica A **390**, 3558 (2011).

[104] P. Zhang, C.-X. Wu, and S. C. Wong, Physica A **391**, 456 (2012).

[105] W.-H. Lee, S.-S. Tseng, J.-L. Shieh, and H.-H. Chen, IEEE Trans. Intell. Transp. Syst. **12**, 1047 (2011).

[106] J.-F. Tian, Z.-Z. Yuan, M. Treiber, B. Jia, and W.-Y. Zhanga, Physica A **391**, 3129 (2012).

[107] R. Borsche, M. Kimathi, and A. Klar, Comput. Math. Appl. **64**, 2939 (2012).

[108] Y. Wang, Y. I. Zhang, J. Hu, and L. Li, Int. J. Mod. Phys. C **23**, 1250060 (2012).

[109] J.-F. Tian, Z.-Z. Yuan, B. Jia, H.-q. Fan, and T. Wang, Phys. Lett. A **376**, 2781 (2012).

[110] H. Yang, J. Lu, X. Hu, and J. Jiang, Physica A **392**, 4009 (2013).

[111] F. Knorr and M. Schreckenberg, J. Stat. Mech. (2013) P07002.

[112] Z.-T. Xiang, Y.-J. Li, Y.-F. Chen, and L. Xiong, Physica A **392**, 5399 (2013).

[113] K. Hausken and H. Rehborn, in *Game Theoretic Analysis of Congestion, Safety, and Security*, Springer Series in Reliability Engineering (Springer, Berlin, 2015), pp. 113–141.

[114] R. Jiang, M.-B. Hu, H. M. Zhang, Z.-Y. Gao, B. Jia, Q.-S. Wu, and M. Yang, PLoS ONE **9**, e94351 (2014).

[115] J. F. Tian, M. Treiber, B. Jia, S. F. Ma, B. Jia, and W. Y. Zhang, Transp. Res. B **71**, 138 (2015).

[116] J. F. Tian, B. Jia, S. F. Ma, C. Q. Zhu, R. Jiang, and Y. X. Ding, Transp. Sci. **51**, 807 (2017).

[117] R. Jiang, M. B. Hu, H. M. Zhang, Z. Y. Gao, B. Jia, and Q. S. Wu, Transp. Res. B **80**, 338 (2015).

[118] J. F. Tian, G. Li, M. Treiber, R. Jiang, N. Jia, and S. F. Ma, Transp. Rec. B **93**, 560 (2016).

[119] J.-F. Tian, R. Jiang, G. Li, M. Treiber, B. Jia, and C. Q. Zhu, Transp. Rec. F **41**, 55 (2016).

[120] J.-F. Tian, R. Jiang, B. Jia, Z.-Y. Gao, and S. F. Ma, Transp. Res. B **93**, 338 (2016).

[121] R. Jiang, C.-J. Jin, H. M. Zhang, Y.-X. Huang, J.-F. Tian, W. Wang, M.-B. Hu, H. Wang, and B. Jia, Transp. Res. Proc. **23**, 157 (2017).

[122] C.-J. Jin, W. Wanga, R. Jiang, H. M. Zhang, H. Wanga, and M.-B. Hud, Transp. Res. C **60**, 324 (2015).

[123] Ch. Xu, P. Liu, W. Wang, and Zh. Li, Accid. Anal. Prev. **85**, 45 (2015).

[124] L. C. Davis, Physica A **451**, 320 (2016).

[125] Because the speed $v$ and space gap $g$ are integer in the discrete version of the TPACC model (5)–(7), the operating points do not form a continuum in the space gap–speed plane as they do in the continuum version of the TPACC model (4).

[126] B. S. Kerner, in *Encyclopedia of Complexity and System Science*, edited by R. A. Meyers (Springer Science+Business Media, Berlin, 2017).

[127] B. S. Kerner, in *Encyclopedia of Complexity and System Science*, edited by R. A. Meyers (Springer Science+Business Media, Berlin, 2018).

[128] The discretization interval of TPACC acceleration (deceleration) made in the TPACC model (5)–(7) is chosen to be an extremely small value that is equal to $\delta a = 0.01$ m/s$^2$ (see Appendix A2). Therefore, the maximum value of a small round-down of $a_n^{(\mathrm{TPACC})}$ in Eqs. (6), (7) through the application of the floor operator $\lfloor a_n^{(\mathrm{TPACC})} \rfloor$ is less than 0.01 m/s$^2$ and it is, therefore, negligible. We have tested that no conclusions about physical features of TPACC dynamic behavior have been changed, when the continuum in space model of human driving vehicles of Ref. [67] and, respectively, the continuum in space TPACC model version (without the the floor operator) is used (the reason for the use of the discrete in space model for human driving vehicles of Ref. [68] that leads to Eqs. (6), (7) has been explained in [68] as well as in Appendix A of [35]).

[129] A more detailed discussion of the application of the three-phase theory for a statistical analysis of traffic stream characteristics (like the definition of "stochastic highway capacity of free flow at a bottleneck" and its theoretical justification made in the three-phase theory) as well as a critical consideration of the three-phase theory [33–35,60,64] versus the classical traffic flow theories and models reviewed in [22–27,29–32] are out of scope of this article: Such a detailed analysis has already been made in the Ref. [35].

[130] Simulations show that even in a nonrealistic case of traffic consisting of 100% of automated driving vehicles the effect of large local speed disturbances at the bottleneck on the overall flow caused by the classical ACC [Figs. 4(a)–4(c)] is also stronger than the effect of the different use of available space on the road by the ACC vehicles and TPACC vehicles. Indeed, under simulation parameters of ACC and TPACC used in Fig. 4, the maximum highway capacity for TPACC vehicles $C_{\mathrm{max,TPACC}} = 2353$ vehicles/h is slightly larger than that for ACC vehicles $C_{\mathrm{max,ACC}} = 2322.6$ vehicles/h.

[131] M. Takayasu and H. Takayasu, Fractals **1**, 860 (1993).

[132] R. Barlović, L. Santen, A. Schadschneider, and M. Schreckenberg, Eur. Phys. J. B **5**, 793 (1998).

[133] S. Krauß, P. Wagner, and C. Gawron, Phys. Rev. E **55**, 5597 (1997).

[134] P. G. Gipps, Trans. Res. B **15**, 105 (1981).

[135] S. Krauß, *Microscopic Modeling of Traffic Flow: Investigation of Collision Free Vehicle Dynamics*, Ph.D. thesis, University of Cologne, Germany (1998), http://e-archive.informatik.uni-koeln.de/319/.

[136] Simulations show that the use of the safe speed in formula (B3) does not influence the dynamics of the ACC vehicles (1) in free flow outside the bottleneck. However, due to vehicles merging from the on-ramp onto the main road, time headway of the vehicle to the preceding vehicle can be considerably smaller than $\tau_{\mathrm{d}}^{(\mathrm{ACC})}$. Therefore, formula (B3) allows us to avoid collisions of the ACC vehicle with the preceding vehicle in such dangerous situations. Moreover, very small values of time headway can occur in congested traffic; formula (B3) prevents vehicle collisions in these cases also. The same conclusion is also valid for TPACC vehicles: The use of the safe speed in formula (7) does not influence the dynamics of the TPACC vehicles (5) in free flow outside the bottleneck. However, formula (7) allows us to avoid collisions of the TPACC vehicle with the preceding vehicle in dangerous situations that can occur at the bottleneck as well as in congested traffic.